TROPOMI validation report of the directionally dependent surface Lambertian-equivalent reflectivity
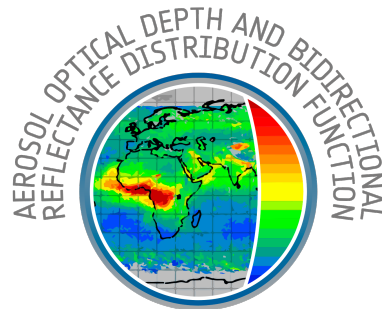
Document approval record

	digital signature
Prepared:	
Checked:	
Approved PM:	
Approved PI:	

Document change record

Issue	Date	Item	Comments
0.0.1	2020-08-26	All	Initial version
0.0.2	2020-09-17	All	Version shared with team (confidential)
0.1.0	2020-11-04	All	Update describing new version 0.4 of the database
1.0.0	2020-11-23		Corrections and update after review:
		5.2.1	- clarified "sufficient cloud free" requirement
		5.4	- clarified "sufficient quality" statement
		7.1	- added reference to statement about phytoplankton and CDOM
1.1.0	2021-05-19	All	Update describing new version 0.5 of the database
1.2.0	2022-01-14	All	Update describing new version 1.0 of the database
2.0.0	2023-09-04		Update describing new version 2.0 of the database:
		3.2	- added a few acronyms to "acronyms and abbreviations"
		5	- updated tables 1 and 2
		7–9	- updated and rewrote sections 7–9; updated all figures
		10	- updated and extended section 10; updated all figures; added figures 25–27
		11	- updated section 11

European Space Agency
Agence spatiale européenne

Contents

European Space Agency
Agence spatiale européenne

List of Tables

List of Figures

1 Introduction

1.1 Identification

This document is identified as S5P-KNMI-L3-0401-RP.

1.2 Purpose and objective

This document is the Validation Report (VR) of the directionally dependent Lambertian-equivalent reflectivity (DLER) of the Earth's surface derived from observations by TROPOMI. The purpose of this VR is to present the validation approach, to present the results from the validation, and to report to the users the quality that they may expect. The document is maintained during the development phase of the data product in the context of the S5p+I project. Several updates of the document are planned.

1.3 Document overview

The structure of this VR is as follows. In section 2 applicable, standard and reference documents are listed. Section 3 introduces terms and definitions used in this VR, along with a list of acronyms and abbreviations that are used throughout the VR. Section 4 provides a reference to a general description of the TROPOMI instrument. Section 5 introduces the heritage surface LER databases that are available for validation. The TROPOMI surface LER and DLER climatologies are also introduced in this section. The validation strategy is outlined in section 6. First the TROPOMI surface LER database is compared to the heritage SCIAMACHY surface LER database in section 7. Then the TROPOMI surface LER database is compared to the heritage OMI surface LER database in section 8. After that, in section 9, the TROPOMI surface LER database is compared to the GOME-2 surface LER database. Finally, the TROPOMI surface DLER is compared to MODIS surface BRDF in section 10. This VR ends with a summary of the validation results in section 11.

European Space Agency
Agence spatiale européenne

2 Applicable and reference documents

2.1 Applicable documents

[AD1] TROPOMI Instrument and Performance Overview.
source: KNMI; **ref:** S5P-KNMI-L2-0010-RP; **issue:** 0.10.0; **date:** 2014-03-15.

2.2 Standard documents

[SD1] Space Engineering – Software.
source: ESA/ECSS; **ref:** ECSS-E-ST-40C; **issue:** 3; **date:** 2009-03-06.

2.3 Reference documents

[RD1] Terms, definitions and abbreviations for TROPOMI L01b data processor.
source: KNMI; **ref:** S5P-KNMI-L01B-0004-LI; **issue:** 3.0.0; **date:** 2013-11-08.

[RD2] Terms and symbols in the TROPOMI Algorithm Team.
source: KNMI; **ref:** S5P-KNMI-L2-0049-MA; **issue:** 2.0.0; **date:** 2016-05-17.

[RD3] R. B. A. Koelemeijer, J. F. de Haan and P. Stammes; A database of spectral surface reflectivity in the range 335–772 nm derived from 5.5 years of GOME observations. *J. Geophys. Res.*; **108** (2003) (D2); doi:10.1029/2002JD002429. URL `https://agupubs.onlinelibrary.wiley.com/doi/abs/10.1029/2002JD002429`.

[RD4] Q. L. Kleipool, M. R. Dobber, J. F. de Haan *et al.*; Earth surface reflectance climatology from 3 years of OMI data. *J. Geophys. Res.*; **113** (2008) (D18); doi:10.1029/2008JD010290. URL `https://agupubs.onlinelibrary.wiley.com/doi/abs/10.1029/2008JD010290`.

[RD5] L. G. Tilstra, O. N. E. Tuinder, P. Wang *et al.*; Surface reflectivity climatologies from UV to NIR determined from Earth observations by GOME-2 and SCIAMACHY. *J. Geophys. Res. Atmos.*; **122** (2017) (7), 4084; doi:10.1002/2016JD025940. URL `https://agupubs.onlinelibrary.wiley.com/doi/abs/10.1002/2016JD025940`.

[RD6] F. E. Nicodemus, J. C. Richmond, J. J. Hsia *et al.*; Geometrical Considerations and Nomenclature for Reflectance. *In Radiometry*; (pp. 94–145) (Jones and Bartlett Publishers, Inc., USA., 1992).

[RD7] L. G. Tilstra, O. N. E. Tuinder, P. Wang *et al.*; Directionally dependent Lambertian-equivalent reflectivity (DLER) of the Earth's surface measured by the GOME-2 satellite instruments. *Atmos. Meas. Tech.*; **14** (2021) (6), 4219; doi:10.5194/amt-14-4219-2021. URL `https://amt.copernicus.org/articles/14/4219/2021/`.

[RD8] D. F. Heath, A. J. Krueger, H. A. Roeder *et al.*; The Solar Backscatter Ultraviolet and Total Ozone Mapping Spectrometer (SBUV/TOMS) for NIMBUS G. *Opt. Eng.*; **14** (1975) (4), 323; doi:10.1117/12.7971839. URL `https://doi.org/10.1117/12.7971839`.

[RD9] J. R. Herman and E. A. Celarier; Earth surface reflectivity climatology at 340–380 nm from TOMS data. *J. Geophys. Res.*; **102** (1997) (D23), 28003; doi:10.1029/97JD02074. URL `https://agupubs.onlinelibrary.wiley.com/doi/abs/10.1029/97JD02074`.

[RD10] J. P. Burrows, M. Weber, M. Buchwitz *et al.*; The Global Ozone Monitoring Experiment (GOME): Mission concept and first scientific results. *J. Atmos. Sci.*; **56** (1999) (2), 151; doi:10.1175/1520-0469(1999)056<0151:TGOMEG>2.0.CO;2. URL `https://doi.org/10.1175/1520-0469(1999)056<0151:TGOMEG>2.0.CO;2`.

[RD11] P. F. Levelt, G. H. J. van den Oord, M. R. Dobber *et al.*; The ozone monitoring instrument. *IEEE Trans. Geosci. Remote Sens.*; **44** (2006) (5), 1093; doi:10.1109/TGRS.2006.872333. URL `https://ieeexplore.ieee.org/document/1624590`.

[RD12] R. Munro, R. Lang, D. Klaes *et al.*; The GOME-2 instrument on the Metop series of satellites: instrument design, calibration, and level 1 data processing – an overview. *Atmos. Meas. Tech.*; **9** (2016) (3), 1279; doi:10.5194/amt-9-1279-2016. URL `https://www.atmos-meas-tech.net/9/1279/2016/`.

[RD13] GOME-2 surface LER product – Algorithm Theoretical Basis Document.
source: KNMI; **ref:** SAF/AC/KNMI/ATBD/003; **issue:** 4.1; **date:** 2023-01-05.

[RD14] H. Bovensmann, J. P. Burrows, M. Buchwitz *et al.*; SCIAMACHY: Mission object-ives and measurement modes. *J. Atmos. Sci.*; **56** (1999) (2), 127; doi:10.1175/1520-0469(1999)056<0127:SMOAMM>2.0.CO;2. URL `https://doi.org/10.1175/1520-0469(1999)056<0127:SMOAMM>2.0.CO;2`.

[RD15] L. G. Tilstra, M. de Graaf, I. Aben *et al.*; In-flight degradation correction of SCIAMACHY UV reflectances and Absorbing Aerosol Index. *J. Geophys. Res.*; **117** (2012) (D6); doi:10.1029/2011JD016957. URL `https://agupubs.onlinelibrary.wiley.com/doi/abs/10.1029/2011JD016957`.

[RD16] TROPOMI ATBD of the directionally dependent surface Lambertian-equivalent reflectivity.
source: KNMI; **ref:** S5P-KNMI-L3-0301-RP; **issue:** 2.0.0; **date:** 2023-08-29.

[RD17] A. Lorente, K. F. Boersma, P. Stammes *et al.*; The importance of surface reflectance anisotropy for cloud and NO_2 retrievals from GOME-2 and OMI. *Atmos. Meas. Tech.*; **11** (2018) (7), 4509; doi:10.5194/amt-11-4509-2018. URL `https://www.atmos-meas-tech.net/11/4509/2018/`.

[RD18] S5p+I – Requirements Baseline Document.
source: KNMI, GRASP, Catalysts; **ref:** D1-RBD; **issue:** 1.0; **date:** 2019-10-09.

[RD19] C. Popp, P. Wang, D. Brunner *et al.*; MERIS albedo climatology for FRESCO+ O_2 A-band cloud retrieval. *Atmos. Meas. Tech.*; **4** (2011) (3), 463; doi:10.5194/amt-4-463-2011. URL `https://www.atmos-meas-tech.net/4/463/2011/`.

[RD20] F. Gao, C. B. Schaaf, A. H. Strahler *et al.*; MODIS bidirectional reflectance distribution function and albedo Climate Modeling Grid products and the variability of albedo for major global vegetation types. *J. Geophys. Res. Atmos.*; **110** (2005), D01104; doi:10.1029/2004JD005190. URL `https://agupubs.onlinelibrary.wiley.com/doi/abs/10.1029/2004JD005190`.

[RD21] G. Lichtenberg, Q. Kleipool, J. M. Krijger *et al.*; SCIAMACHY Level 1 data: calibration concept and in-flight calibration. *Atmos. Chem. Phys.*; **6** (2006) (12), 5347; doi:10.5194/acp-6-5347-2006. URL `https://www.atmos-chem-phys.net/6/5347/2006/`.

[RD22] GOME-2 surface LER product – Validation Report.
source: KNMI; **ref:** SAF/AC/KNMI/VR/002; **issue:** 1/2023; **date:** 2023-01-05.

[RD23] MODIS BRDF/Albedo Product: Algorithm Theoretical Basis Document.
source: MODIS Science Team; **ref:** MODIS Product ID: MOD43; **issue:** 5.0; **date:** April 1999.

[RD24] L. G. Tilstra, M. de Graaf, P. Wang *et al.*; In-orbit Earth reflectance validation for TROPOMI on board the Sentinel-5 Precursor satellite. *Atmos. Meas. Tech.*; **13** (2020) (8), 4479; doi:10.5194/amt-13-4479-2020. URL `https://amt.copernicus.org/articles/13/4479/2020/`.

[RD25] W. Wanner, X. Li and A. H. Strahler; On the derivation of kernels for kernel-driven models of bidirectional reflectance. *J. Geophys. Res.*; **100** (1995) (D10), 21077; doi:10.1029/95JD02371. URL `https://agupubs.onlinelibrary.wiley.com/doi/abs/10.1029/95JD02371`.

[RD26] J.-L. Roujean, M. Leroy and P.-Y. Deschamps; A bidirectional reflectance model of the Earth's surface for the correction of remote sensing data. *J. Geophys. Res.*; **97** (1992) (D18), 20455; doi:10.1029/92JD01411. URL `https://agupubs.onlinelibrary.wiley.com/doi/abs/10.1029/92JD01411`.

[RD27] X. Li and A. H. Strahler; Geometric-optical bidirectional reflectance modeling of a conifer forest canopy. *IEEE Trans. Geosci. Remote Sens.*; **GE-24** (1986) (6), 906; doi:10.1109/TGRS.1986.289706.

2.4 Electronic references

[ER1] URL `https://www.temis.nl/surface/albedo/toms_ler.php`.

[ER2] URL `https://www.temis.nl/surface/albedo/gome_ler.php`.

[ER3] URL `https://www.temis.nl/surface/albedo/omi_ler.php`.

[ER4] URL `https://www.temis.nl/surface/albedo/scia_ler.php`.

[ER5] URL `https://www.temis.nl/surface/albedo/gome2_ler.php`.

[ER6] URL `https://lpdaac.usgs.gov/products/mcd43c2v061/`.

3 Terms, definitions and abbreviated terms

Terms, definitions and abbreviated terms that are used in the documentation of the TROPOMI L0-1b data processor are described in [RD1]. Terms, definitions and abbreviated terms for TROPOMI Level 2 algorithms are described in [RD2]. Terms, definitions and abbreviated terms specific for this document are defined below.

3.1 Terms and definitions

There are no document specific terms and definitions.

3.2 Acronyms and abbreviations

AAI	Absorbing Aerosol Index
ATBD	Algorithm Theoretical Baseline Document
BRDF	Bidirectional Reflectance Distribution Function
BSA	Black-Sky Albedo
CAMS	Copernicus Atmosphere Monitoring Service
CF	Climate and Forecast metadata conventions
DAK	Doubling-Adding KNMI
DARIUS	Development of Advanced Retrieval of Aerosol and Surface Properties from S5P
DLER	Directionally dependent Lambertian-Equivalent Reflectivity
DU	Dobson Units, 2.69×10^{16} molecules cm^{-2}
ECMWF	European Centre for Medium-Range Weather Forecast
ENVISAT	Environmental Satellite
EOS-Aura	Earth Observing System – Aura satellite
EPS-SG	EUMETSAT Polar System – Second Generation
ERS	European Remote Sensing Satellite
ESA	European Space Agency
EUMETSAT	European Organisation for the Exploitation of Meteorological Satellites
FOV	Field-of-View
FRESCO	Fast Retrieval Scheme for Clouds from the Oxygen A band
GMTED2010	Global Multi-resolution Terrain Elevation Data 2010
GOME	Global Ozone Monitoring Experiment
GRASP	Generalized Retrieval of Atmosphere and Surface Properties
HDF	Hierarchical Data Format
HITRAN2008	High-Resolution Transmission molecular absorption database, 2008 edition
IR	Infrared
ISRF	Instrument Spectral Response Function
KNMI	Koninklijk Nederlands Meteorologisch Instituut
LER	Lambertian-Equivalent Reflectivity
LUT	Look-Up Table
L2OP	Level-2 Operational Processor
L2PP	Level-2 Prototype Processor
MERIS	Medium Resolution Imaging Spectrometer
METOP	Meteorological Operational Satellite
MLS	Mid-Latitude Summer
NASA	National Aeronautics and Space Administration
NETCDF	Network Common Data Form, NetCDF
NIR	Near-Infrared

NISE	Near-real-time Ice and Snow Extent
NRT	Near-Real-Time
OMI	Ozone Monitoring Instrument
RAA	Relative Azimuth Angle
RMSE	Root-Mean-Square Error
RTM	Radiative Transfer Model
SAA	Solar Azimuth Angle
SCIAMACHY	Scanning Imaging Absorption Spectrometer for Atmospheric Chartography
Suomi NPP	Suomi National Polar-orbiting Partnership
SW	Software
SWIR	Short-Wavelength Infrared
SZA	Solar Zenith Angle
S5	Sentinel-5 mission
S5P	Sentinel-5 Precursor mission
TBA	To be Added
TBC	To be Confirmed
TBD	To be Defined
TOA	Top-of-Atmosphere
TOMS	Total Ozone Mapping Spectrometer
TROPOMI	Tropospheric Monitoring Instrument
UTC	Coordinated Universal Time
UV	Ultraviolet
UVNS	Ultraviolet Visible Near-infrared Shortwave spectrometer
VAA	Viewing Azimuth Angle
VIIRS	Visible Infrared Imaging Radiometer Suite
VIS	Visible
VZA	Viewing Zenith Angle

4   TROPOMI instrument description

A description of the TROPOMI instrument and performance can be found in [AD1].

5 Introduction to the TROPOMI DLER database

5.1 Background

Surface reflectivity databases are needed for cloud, aerosol and trace gas retrievals. Examples are the retrieval of trace gases such as ozone, NO_2, BrO, CH_2O, H_2O, CO_2, CO, and CH_4, and of cloud information and aerosol optical depth. The TROPOMI surface DLER product is the directionally dependent Lambertian-equivalent reflectivity (LER) of the Earth's surface observed by TROPOMI. It is the improved follow-up of earlier surface LER databases based on observations performed by GOME-1 (on ERS-2) [RD3], OMI (on the Aura satellite) [RD4], as well as SCIAMACHY (on Envisat) and GOME-2 (on the MetOp satellites) [RD5]. In this chapter, the term "surface reflectivity database" refers to global climatologies of surface albedo, available for several wavelength bands and for each month. The databases are generally extracted from several years of data and the term "surface reflectivity database" therefore always refers to a L4 product.

5.2 Heritage

The heritage from the traditional surface LER databases is described in section 5.2.1. These databases adhere to the principle of Lambertian surface reflection, which means that they completely disregard the fact that surface reflection is described by a bi-directional reflectance distribution function (BRDF) [RD6] which takes into account the dependence on the incoming and outgoing directions of the light reflected by the surface. Lambertian surface reflection is by definition non-directional. A directionally dependent LER (acronym: DLER) was first derived for the GOME-2 instrument [RD7]. This database will be discussed in section 5.2.2.

5.2.1 Lambertian-equivalent reflectivity (LER) databases

One of the first surface reflectivity databases retrieved using UV satellite remote sensing techniques is the Total Ozone Mapping Spectrometer (TOMS) [RD8] surface LER database [RD9]. The retrieved reflectivity is the so-called Lambertian-equivalent reflectivity (LER) of the surface found from scenes which are assumed to be cloud free. The retrieval method relies on the removal of the (modelled) atmospheric contribution from the (observed) top-of-atmosphere (TOA) reflectance. In this approach the surface is defined to behave as a Lambertian reflector. The TOMS surface LER database, which is provided in a spatial grid of $1.25° \times 1.0°$, was retrieved for 340 and 380 nm only, which severely limits its usefulness.

The GOME-1 [RD10] surface reflectivity database provides the surface LER on a $1.0° \times 1.0°$ grid for 11 wavelength bands between 335 and 772 nm [RD3]. Although this is already quite an improvement with respect to the TOMS surface LER database, the database is still limited in quality by the low number of measurements from which the surface LER had to be extracted and the large GOME footprint size (see Table 1). In particular, pixels over sea are often affected by residual cloud contamination. In these cases the surface LER was retrieved from scenes which were not sufficiently cloud free, evidenced by LER values at 772 nm exceeding 0.05 [RD3]. In other cases, e.g. snow surfaces, the surface LER was retrieved from a few measurements which were not representative for the entire month.

A large improvement on these points is the OMI surface reflectivity database [RD4]. First, the OMI instrument [RD11] has a much smaller footprint size (24 $\times$ 13 km^2 at nadir) combined with a larger global coverage (see Table 1). This leads to better statistics and results in a higher accuracy for the surface LER retrieval. Second, the higher number of measurements allows for inspecting the distribution of scene LERs for each grid cell, and for making a more sophisticated selection of representative (cloud-free) scenes instead of directly taking the minimum scene LER value like in the case of the TOMS and GOME-1 databases. Third, the provided OMI surface LER database has a higher spatial resolution of $0.5° \times 0.5°$. The limiting factor is the OMI wavelength range. The longest wavelength in the OMI surface LER database is 499 nm.

The GOME-2 series of satellite instruments [RD12] does not have the limitations of the above instruments and therefore can be used to create a better surface LER database. The GOME-2 instrument has the spectral range of GOME but a much smaller footprint (80 $\times$ 40 km^2) which is constant over the full swath width. The number of measurements that are available per longitude/latitude cell in the database grid is smaller than that of OMI, but enough to perform a statistical analysis on the distribution of retrieved scene LERs. The intrinsic spatial resolution of the GOME-2 surface LER database is $1.0° \times 1.0°$ [RD5], except near the coastlines and for certain region such as snow covered mountain ranges where it is $0.25° \times 0.25°$ [RD7, RD13].

The SCIAMACHY instrument [RD14] is comparable to the GOME-2 instrument, but covers a much larger spectral range. The derived SCIAMACHY surface LER database offers 34 wavelength bands between 328 and 2314 nm [RD5]. The main advantage of the GOME-2 and SCIAMACHY surface LER databases with respect

European Space Agency
Agence spatiale européenne

Surface LER database →	TOMS	GOME-1	OMI	SCIAMACHY	GOME-2	Sentinel-5P
surface reflectivity type	LER	LER	LER	LER	LER / DLER	LER / DLER
dataset time range [1]	1978–1993	1995–2000	2004–2007	2002–2012	2007→	2018→
selected wavelength bands	2	11	23	34	27	21
wavelength range covered [nm]	340–380	335–772	328–499	328–2314	328–772	328–2314
band width [nm]	1.0	1.0	1.0	1.0	1.0	1.0
spatial resolution [°lon × °lat]	1.25 × 1.0	1.0 × 1.0	0.5 × 0.5	0.5 × 0.5 [2]	0.25 × 0.25 [2]	0.125 × 0.125
reference	[RD9]	[RD3]	[RD4]	[RD5]	[RD5, RD7]	[RD16]
instrument	TOMS	GOME	OMI	SCIAMACHY	GOME-2	TROPOMI
satellite	Nimbus-7	ERS-2	Aura	Envisat	MetOp-A/B/C	Sentinel-5P
equator crossing time (LT)	12:00	10:30	13:45	10:00	09:30	13:30
dayside flight direction	S→N	N→S	S→N	N→S	N→S	S→N
number of days for global coverage	1	3	1	6	1.5	1
pixel size at nadir [km × km]	50 × 50	320 × 40	24 × 13	60 × 30	80 × 40	5.6 × 3.6 [3]
number of usable pixels per orbit	∼12000	∼1300	∼83000	∼4000	∼11000	∼1300000

Table 1: Characteristics and properties of the surface LER databases, and of the satellite instruments from which they are derived. Wavelength band information can be found in Table 2.

to the OMI surface LER database is the wider wavelength range of the GOME-2 and SCIAMACHY instrument. Additionally, the retrieval algorithm uses aerosol information, available via the Absorbing Aerosol Index (AAI) product [RD15], to filter out scenes with large amounts of aerosols, as these scenes can result in inaccurate values of the retrieved surface LER. This filtering is especially important for locations over desert areas.

The SCIAMACHY and GOME-2 surface LER databases are derived by similar retrieval codes using similar techniques. Together with the OMI surface LER database they provide all the heritage available to develop the TROPOMI surface DLER database. Table 1 summarises the properties of the surface reflectivity databases discussed in this section. References to papers and other sources of information are also provided. Table 2 provides detailed information on the wavelength bands that are contained in the surface LER databases.

5.2.2 Directional LER databases

The concept of a directional LER was first introduced to the GOME-2 surface DLER database [RD7]. The GOME-2 surface DLER database provides, next to the traditional LER database, a DLER database which is essentially a function of the viewing direction (and of month, wavelength, latitude, and longitude). For the GOME-2 surface DLER database, the difference between DLER and LER is the largest for the west viewing geometries. For example, at 772 nm the surface DLER for a vegetated scene over Amazonia can be twice as large in the west viewing direction as in the east viewing direction [RD17]. The traditional LER databases discussed in section 5.2.1 completely miss this directional dependence, and generally present a value which is very close to the minimum of the DLER over all viewing angles.

5.2.3 Links to the heritage LER databases

The heritage LER databases can be download from the following locations:

– TOMS surface LER   :   [ER1]

– GOME-1 surface LER   :   [ER2]

– OMI surface LER   :   [ER3]

– SCIAMACHY surface LER   :   [ER4]

– GOME-2 surface DLER   :   [ER5]

---

[1] The longer the time period, the larger the number of times a certain region has been observed. This increases the chances of having observed this region under clear-sky conditions.   [2] The *intrinsic* resolution is in most cases $1.0° \times 1.0°$.   [3] The TROPOMI spatial sampling in the along track direction was changed from 7.2 km to the indicated 5.6 km on 6 August 2019, at the start of orbit 9388.

5.3   TROPOMI DLER database

The TROPOMI surface DLER database is in many aspects a huge step forward compared to the other databases described in Table 1. The spatial resolution of the TROPOMI DLER database will be $0.125° \times 0.125°$. This high spatial resolution is made possible by the small TROPOMI footprint size of 5.6×3.6 km^2. The smaller footprint size also results in a much larger number of cloud-free pixels that may be collected over the course of a given time period. This is beneficial for the stability and the quality of the retrieved DLER spectra. Figure 1 provides a good indication of the spatial resolution for the surface LER climatologies derived from GOME-1, GOME-2, and TROPOMI. Obviously, the higher spatial resolution of TROPOMI is an important improvement.
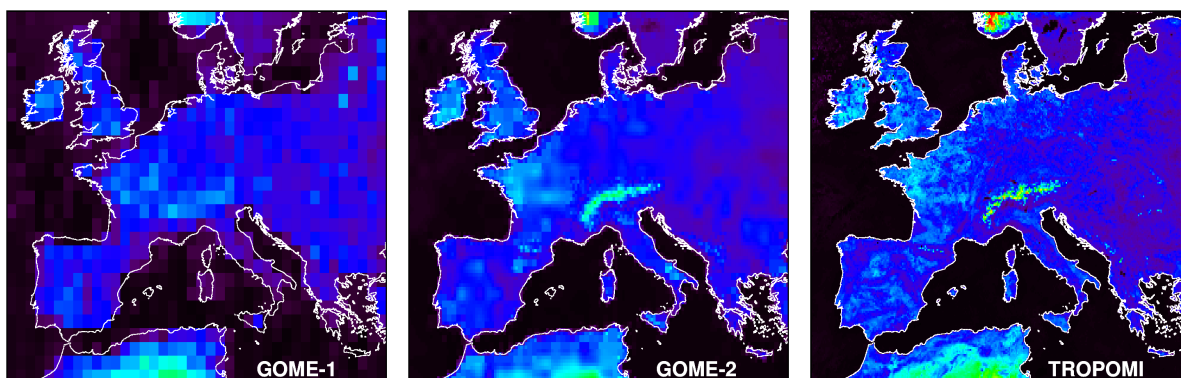
Figure 1: Surface LER in March over Europe according to the GOME-1, GOME-2, and TROPOMI databases.

Another step forward is the way in which the cloud screening is performed. For all surface LER databases listed in Table 1 the cloud screening is based on statistical methods. The advantage of this is that external cloud information is not required. The disadvantage is the risk of residual cloud contamination for areas known to be nearly always covered by persistent cloud decks. Another disadvantage is the high computational effort needed: all scenes need to be handled at once, cloud-free or not, which can be quite a task when handling a satellite instrument like TROPOMI with more than a million footprints per orbit (see Table 1).

For TROPOMI the cloud screening will be based primarily on the S5P NPP-VIIRS cloud product. The NPP-VIIRS product is based on observations performed by the VIIRS instrument onboard the Suomi NPP satellite. The S5P and NPP satellites are kept in a "loose" formation in very similar orbits, resulting in only a relatively small time difference (currently the difference is approximately 3 minutes, reduced from 5 minutes at the start of the mission). The VIIRS cloud information is provided for each individual TROPOMI footprint. More precisely, the product provides cloud information for four sets of boxes surrounding the TROPOMI measurement footprint. For our purpose, we use the nominal size of these boxes, corresponding to the smallest FOV, which matches precisely the size of the TROPOMI footprints as found in the L1 and L2 products. Separate S5P NPP-VIIRS products are provided for spectral band 3, 6, and 7. This means that there is collocated cloud information available for all used TROPOMI spectral bands (these are: bands 3/4, 5/6, and 7).

Another major improvement is in the fact that for determining the TROPOMI surface DLER, the information can be studied as a function of viewing angle without the use of viewing-angle containers. For the GOME-2 DLER, these viewing-angle containers are needed to be able to perform the statistical cloud screening [RD7]. The fact that the "container" approach is not needed for deriving the TROPOMI surface DLER is, therefore, a direct result of the decision to use the S5P NPP-VIIRS cloud product for the cloud screening.

Generally speaking, the approach that was used for the GOME-2 and SCIAMACHY surface reflectivity databases was followed closely and applied in the TROPOMI surface DLER retrieval algorithm.

5.4   Wavelength bands

In Table 2 we list the wavelength bands of the surface reflectivity databases discussed in section 5.2, and their application. As can be seen, the selection of the wavelength bands for TROPOMI was influenced largely by the already existing surface LER databases. Below 325 nm the surface contribution to the TOA reflectance is low, which prevents an accurate retrieval of the surface LER below this wavelength. The TROPOMI surface LER wavelength band at 328 nm is retrieved, but for the time being only for testing and monitoring purposes. It will not be part of the TROPOMI surface DLER database unless it is proven to be of sufficient quality. Sufficient quality means that the requirements set in the Requirements Baseline Document [RD18] need to be met.

Band	TOMS	GOME	OMI	SCIAMACHY	GOME-2	TROPOMI	Application
328			+ [1]	+ [1]	+ [1]	+ [1]	ozone, HCHO, SO_2
335		+	+	+	+	+	ozone, HCHO
340	+			+	+	+	cloud, aerosol, HCHO, BrO
342			+				cloud, aerosol, HCHO, BrO
345			+				cloud, aerosol, HCHO, BrO
354			+	+	+	+	cloud, aerosol, HCHO, BrO, OClO
367			+	+	+	+	cloud, aerosol, OClO
372			+				cloud, aerosol, OClO
376			+				cloud, aerosol, OClO
380	+	+	+	+	+	+	cloud, aerosol, OClO
388			+	+	+	+	cloud, aerosol, OClO
402						+	cloud, aerosol
406			+				cloud, aerosol
416		+	+		+	+	cloud, aerosol
418			+				cloud, aerosol
425			+	+	+	+	cloud, aerosol, NO_2
440		+	+	+	+	+	cloud, aerosol, NO_2
442			+				cloud, aerosol, NO_2
452			+				cloud, aerosol, NO_2
463		+	+	+	+	+	cloud, aerosol, NO_2, O_2-O_2
471			+				cloud, aerosol, NO_2, O_2-O_2
477			+ [2]				cloud, aerosol, NO_2, O_2-O_2
488			+				cloud, aerosol, NO_2, O_2-O_2
494		+	+	+	+	+	cloud, aerosol, NO_2, O_2-O_2
499			+				cloud, aerosol
510				+	+		cloud, aerosol
526				+	+		cloud, aerosol
546				+	+		cloud, aerosol
555		+		+	+		cloud, aerosol
564				+	+		cloud, aerosol, O_2-O_2
585				+			cloud, aerosol, O_2-O_2, H_2O
610		+			+		cloud, aerosol, H_2O
614				+			cloud, aerosol, H_2O
640				+	+		cloud, aerosol, H_2O
670		+		+	+	+	cloud, aerosol, H_2O, O_2-B
685				+	+	+	cloud, aerosol, H_2O, O_2-B
697				+	+	+ [3]	cloud, aerosol, H_2O, O_2-B
712				+	+	+ [3]	cloud, aerosol, H_2O, O_2-B
747				+	+		cloud, aerosol, H_2O
758		+		+	+	+	cloud, aerosol, O_2-A
772		+		+	+	+	cloud, aerosol, O_2-A
862				+			cloud, aerosol, H_2O
875				+			cloud, aerosol, H_2O

1030				+			cloud, aerosol, H_2O
1053				+			cloud, aerosol, H_2O
1245				+			cloud, aerosol, H_2O
1557				+			cloud, aerosol, H_2O, CH_4, CO_2
1593				+			cloud, aerosol, H_2O, CH_4, CO_2
1630				+			cloud, aerosol, H_2O, CH_4, CO_2
1670				+			cloud, aerosol, H_2O, CH_4, CO_2
2314				+		+ [4]	cloud, aerosol, H_2O, CH_4, CO

Table 2: Wavelength bands of the surface LER databases discussed in this paper, and their atmospheric applications. All wavelength bands are located outside strong gaseous absorption bands in order to avoid complicated modeling of the radiative transfer involved. The wavelength bands are 1 nm wide in most cases.

For most of the wavelength bands the exact central wavelength is not very critical, and the exact central position in the algorithm setup is exactly that as shown in Table 2. Exceptions are the 697 and 712-nm TROPOMI DLER wavelength bands. These have been given a central wavelength of 696.97 and 712.70 nm, respectively. The positions of these wavelength bands are based on very precise spectral calculations with the goal to minimise the impact of surrounding water vapour absorption bands. The width of the wavelength bands will be one nm in most cases. Exceptions are the wavelength bands at 697, 712, and 2314 nm. The 697 and 712-nm wavelength bands will have a bandwidth of 0.3 nm. The 2314-nm wavelength band will have a bandwidth of 0.5 nm. The bandwidths that are defined for TROPOMI are in line with those used in the earlier databases.

---

[1] Retrieval of the surface LER below 330 nm is challenging because of the small contribution of the surface to the TOA reflectance.
[2] The wavelength band at 477 nm is ill-positioned because here the retrieved (OMI) surface LER is affected by O_2-O_2 absorption. [3] The 697 and 712-nm wavelength bands are surrounded by water vapour absorption bands. Their bandwidth is 0.3 nm and their exact positions are 696.97 and 712.70 nm, respectively. [4] The 2314-nm wavelength band will have a bandwidth of 0.5 nm.

European Space Agency
Agence spatiale européenne

6 Validation strategy

6.1 LER: comparison with heritage databases

Validation of the retrieved TROPOMI surface LER database may be performed by comparison with the other surface LER databases that were discussed in section 5.2.1. From these databases, the SCIAMACHY surface LER database [RD5] makes most sense as a reference for the TROPOMI surface LER database, because of the largely overlapping set of surface LER wavelength bands, and because it makes use of a similar surface LER retrieval approach as the one described in this ATBD. The GOME-2 surface LER database [RD5] is also created using the same retrieval approach and is therefore also well suitable as a reference.

The OMI surface LER database [RD4] may be used as a reference for the wavelengths below 500 nm. The retrieval algorithm that was used for the OMI surface LER database is comparable to the algorithm used for the TROPOMI surface LER. Moreover, the OMI instrument has a local equator crossing time (13:45 LT) which is close to TROPOMI's (13:30 LT). This is certainly an advantage because it ensures that the solar angles for TROPOMI and OMI are similar. As a result, surface BRDF effects are also similar.

The GOME-1 surface LER database [RD3] unfortunately is fairly outdated and is suffering much more than the other databases from measurement errors, residual cloud contamination, and the effects of instrument degradation. As a result, its quality is lower than that of the other heritage databases [RD5], making it a less reliable reference. It also offers only a rather limited number of wavelength bands for comparison. As a result, comparing with the GOME-1 database does not seem worth the effort.

A comparison with non-Lambertian surface albedos, such as the MERIS black-sky albedo (BSA) [RD19], is in principle also possible. This is strictly speaking not correct, because the BSA is the integral of the bidirectional reflectance distribution function (BRDF) over the entire hemisphere whereas the LER is derived from the much smaller range of viewing angles of the satellite's observation geometry. Note that a comparison with the MERIS BSA database would only make sense over land, because the MERIS surface albedo values over sea are not retrieved from MERIS observations. They were taken directly from the GOME-1 surface LER database [RD19]. Comparisons between SCIAMACHY and MERIS surface albedo databases suggest that a comparison with the MERIS BSA is indeed not worth the effort [RD5].

In summary, for the TROPOMI surface LER product it makes most sense to perform the validation by comparison with the SCIAMACHY, OMI, and GOME-2 surface LER databases. The results of these three database intercomparisons are discussed in sections 7, 8, and 9, respectively.

6.2 DLER: comparison with MODIS BRDF

For the directional TROPOMI surface DLER the only sensible form of validation is a comparison with one of the established MODIS surface BRDF products [RD20]. For that we select the MCD43C2 v6.1 product [ER6]. The spatial resolution of this product is $0.05° \times 0.05°$. The available MODIS wavelength bands are 469, 555, 645, 859, 1240, 1640, and 2130 nm. This means, that more or less exact comparisons are only possible for the 463-nm wavelength band and – to a lesser degree – the 670-nm wavelength band. For the other bands the wavelength differences between the TROPOMI surface DLER and MODIS surface BRDF wavelength bands are simply too large (see Table 2). The directional dependence of the TROPOMI DLER can therefore only be checked in a qualitative way. The MCD43C2 product only provides BRDF coefficients over land. The results of the comparison with MODIS BRDF are presented in section 10.

6.3 Comparison with previous versions of the database

The version of the database under validation is version 2.0. Improvements can be followed by comparison with the previous version of the database (in this case the previous database version is version 1.0).

7 TROPOMI versus SCIAMACHY

In this section, we compare the TROPOMI surface LER product with the SCIAMACHY surface LER product. The orbital parameters for TROPOMI and OMI are quite different (see Table 1) which makes the comparison less than ideal from this point of view. Also, the time periods covered by the two database are very different (TROPOMI: 2018–2023; SCIAMACHY: 2002–2012). On the other hand, the retrieval algorithms are comparable and the SCIAMACHY surface LER database covers the wavelength range 328–2314 nm, so we can analyse nearly all wavelength bands contained in the TROPOMI surface LER database.

7.1 Global maps of the differences

For each month of the year and for each wavelength band in the TROPOMI surface LER database (see Table 2) we calculate the difference in surface LER provided by the TROPOMI and SCIAMACHY surface LER databases. A typical outcome is shown in Figure 2, which presents a global map of the surface LER difference for the 758-nm wavelength band for the month March. Over the ocean the agreement is generally very good. Some mild features related to cloud contamination are visible, most likely caused by the SCIAMACHY surface LER database because the features are blue. Note that the TROPOMI surface LER database is currently based on five years of mission data. As a result, signs of cloud contamination should be scarce, also because the post-processing correction for cloud contamination should remove the strongest remaining cases of cloud contamination. Over land the TROPOMI surface LER is in many cases higher than the SCIAMACHY surface LER. This happens mostly for the deserts, where the surface albedo is higher than for vegetated surfaces. The differences over deserts can go up to 0.04. This difference might be explained by the difference in overpass time between TROPOMI and SCIAMACHY, leading to a different solar geometry and a different BRDF.

There are quite a few regions where the surface LER difference is found to be negative (indicated by the blue areas in Figure 2). In Equatorial Africa this might point to less residual cloud contamination in the TROPOMI surface LER database. This is a region known for a high likelihood of cloud cover. It could be that for this region the TROPOMI surface LER database does a better job than the SCIAMACHY surface LER database. The smaller footprint size of TROPOMI is probably the reason for this, but it can also be a result of the difference in overpass times. Cloud presence can exhibit quite a large diurnal cycle. Also in North and South America some blue features are seen. Note that all blue areas are vegetated surfaces. The differences might also be caused by a difference in BRDF due to the differences in solar position. Indeed, the BRDF for vegetated surfaces is strongly dependent on the viewing and solar geometry.

In Figure 3 we present the same type of plot for the same month of the year (March) but now for the 494-nm wavelength band. For this wavelength band the agreement between the TROPOMI and SCIAMACHY surface LER appears to be better. Over the ocean the absolute difference is comparable to that at 758 nm and well within the 0.01 level, despite the fact that the ocean surface LER at 494 nm is normally larger than at 758 nm. As before, red features, if present, could be related to cloud contamination in the TROPOMI surface LER. Over land, the biases found earlier at 758 nm are not present. The agreement at 494 nm seems to be much better than at 758 nm, but this may also be caused by the fact that the surface LER values over land are also typically lower at 494 nm than what they are at 758 nm.

The comparison for the 380-nm wavelength band is presented in Figure 8. At 380 nm the surface albedo values of land and water are comparable and this is reflected in the results. Over land the agreement is quite good. The differences over ocean are typically found between –0.02 and 0. The blue patterns over the ocean are most likely caused by cloud contamination in the SCIAMACHY surface LER database. If this explanation is true, then the TROPOMI surface LER database is quite accurate at 380 nm for both land and ocean. Please note that previous versions of the TROPOMI surface LER database (up to version 1.2) showed a large positive bias in the UV and at 380 nm. This bias was caused by radiometric calibration problems in TROPOMI spectral bands 3 and 4. These issues are solved in the reprocessed collection-3 TROPOMI data that were used to generate the TROPOMI surface DLER database.

Figure 5 presents the comparison for 2314 nm. The 2314-nm wavelength band of the SCIAMACHY surface LER database was retrieved from SCIAMACHY band 8. This band was troubled by the build up of an ice layer on the detector, and by the many attempts to remove this ice layer by heating up the detector [RD21]. This had an impact on the throughput of the detector. Corrections were made to handle these issues, but the quality of the 2314-nm band in the SCIAMACHY surface LER database cannot be guaranteed. Still, the SCIAMACHY surface LER database is the only heritage database that contains this wavelength band, so we have no alternative. Over the ocean, the agreement between the TROPOMI surface LER database and the SCIAMACHY surface LER database is excellent. Over land, there are some large areas where the agreement

TROPOMI (758 nm) – SCIAMACHY (758 nm)

Figure 2: Map of the difference between the 758-nm surface LER from the TROPOMI and SCIAMACHY surface LER databases. Over the ocean, the agreement is very good. Over land, TROPOMI shows values higher up to about 0.04 over the deserts and lower down to about 0.04 over vegetated regions.

TROPOMI (494 nm) – SCIAMACHY (494 nm)

Figure 3: Map of the difference between the 494-nm surface LER from the TROPOMI and SCIAMACHY surface LER databases. Over the ocean, the agreement is very good, and over land the agreement is good and much better than at 758 nm (see Figure 2).

European Space Agency
Agence spatiale européenne

TROPOMI (380 nm) − SCIAMACHY (380 nm)

MIN-LER

MARCH

-0.08   -0.06   -0.04   -0.02   0.00   0.02   0.04   0.06   0.08

Figure 4: Map of the difference between the 380-nm surface LER from the TROPOMI and SCIAMACHY surface LER databases. The blue colour over the ocean can be attributed to cloud contamination in the SCIAMACHY surface LER database. Agreement is good over both land and ocean.

TROPOMI (2314 nm) − SCIAMACHY (2314 nm)

MIN-LER

MARCH

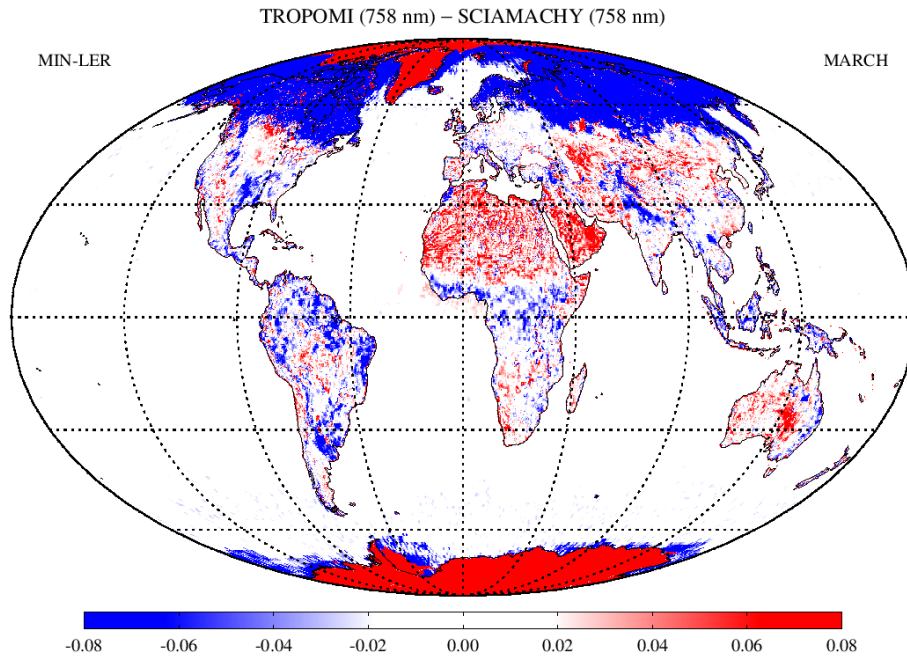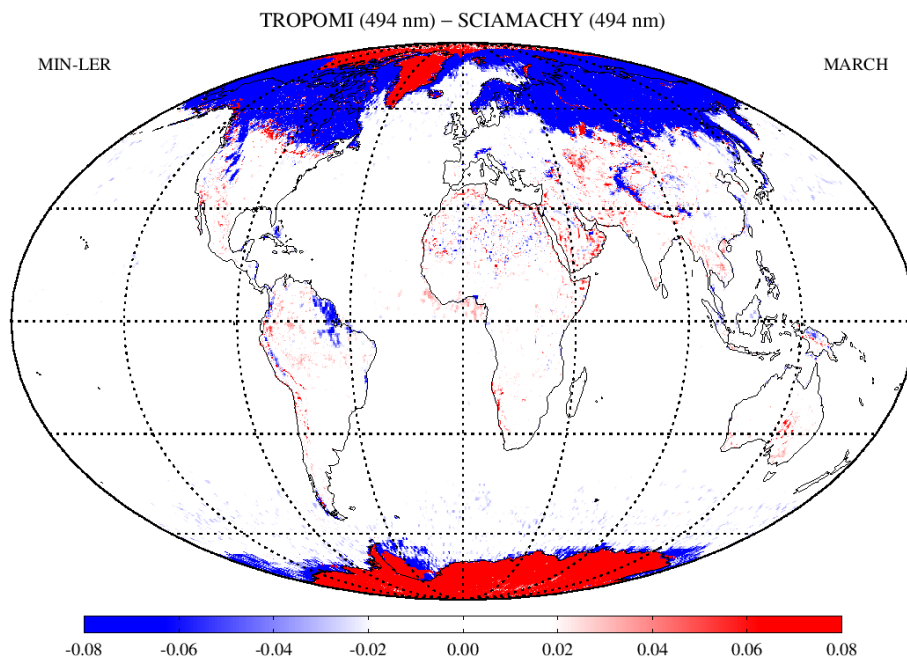-0.08   -0.06   -0.04   -0.02   0.00   0.02   0.04   0.06   0.08

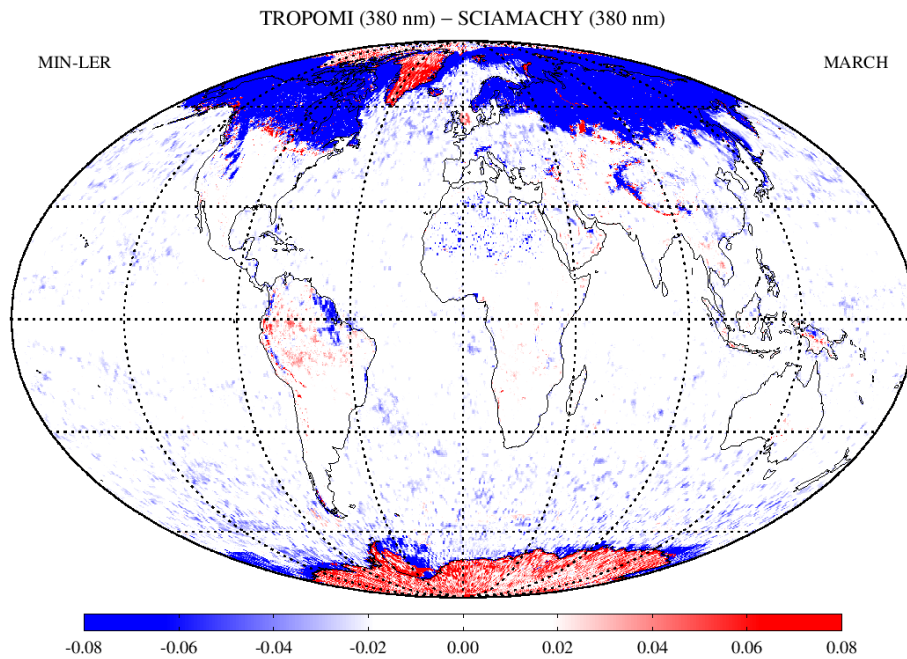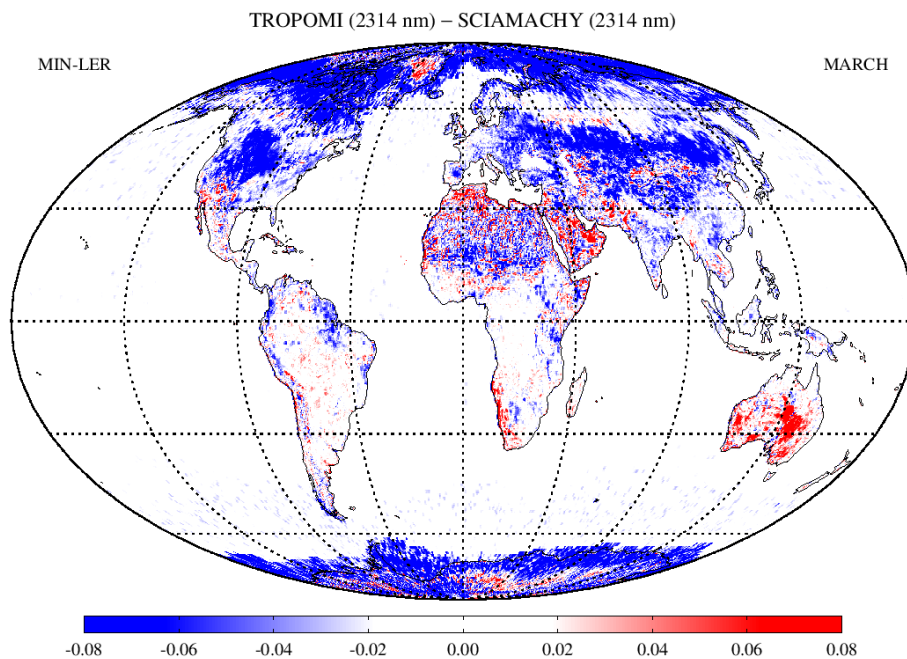**Figure 5**: Map of the difference between the 2314-nm surface LER from the TROPOMI and SCIAMACHY surface LER databases. Over the ocean, the agreement is excellent. Over land, the agreement is fair. A blue colour dominates for desert and snow/ice regions. In certain regions, a red colour dominates.

European Space Agency
Agence spatiale européenne

is good. There are also quite a few areas where a negative bias is found. This happens mostly for desert and snow/ice surfaces. Given the issues related to SCIAMACHY band 8, it is hard to draw conclusions.

7.2 Statistical analysis of the differences

To provide a more statistical analysis of the differences between the TROPOMI and SCIAMACHY surface LER databases, we present in Figures 6 to 9 histograms of the surface LER differences that were found. We only consider surface LER data with latitudes between 60°N and 60°S, thereby excluding data measured for extreme solar zenith angles as well as data located near the polar regions. Snow/ice surfaces are not actively removed from the comparison. The black histograms represent all possible scenes, the blue histograms are based on scenes over water, the green histograms are based on scenes over land and/or snow/ice. The histograms are provided for each calendar month. The mean of the distribution is represented by the dashed vertical line, the mode of the distribution is given by the dotted vertical line.

Figure 6 presents the result for the 758-nm wavelength band. The results indicate a good agreement between the TROPOMI and SCIAMACHY surface LER database at this wavelength. The distributions are symmetric, and the mean bias is very close to zero. This is the case for all months. Additionally, the histograms of land and ocean are very similar in shape. The accuracy requirement of 0.02 in the surface LER seems to be met easily. In Figure 7 the results for the 494-nm wavelength band are presented. There is good agreement and the histograms are only slightly asymmetric. This is mostly the case for the "water" histograms. The asymmetry seems to depend slightly on the calendar month. For instance, in May to July the asymmetry is quite large. Also at 494 nm the accuracy requirements are easily met.

In Figure 8 the histograms for the 380-nm wavelength band are presented. The bias in the TROPOMI surface LER is negative and about –0.01, somewhat depending on the month. Small differences between land and ocean are found, land performing a bit better than ocean. This may very well be related to cloud contamination present in the SCIAMACHY surface LER database. The slight asymmetry in the "water" distributions that was found for the 494-nm wavelength band is not present at 380 nm.

Finally, in Figure 9 we present the histograms for the 2314-nm wavelength band. Over the ocean, the agreement between TROPOMI and SCIAMACHY surface LER is very good. It should be noted, though, that the surface albedo over the ocean is very low at this wavelength (typically below 0.01). It is therefore no real surprise that there is a good agreement. Over land, the distributions are rather asymmetric for some of the months (e.g. October). The change in the asymmetry from one month to another is connected to the presence of snow/ice in the one month and the absence of snow/ice in the other. As snow and ice surfaces generally have a large surface LER ($\sim$0.8), the differences between TROPOMI and SCIAMACHY due to calibration errors will also be large. If snow/ice is absent, then lower values are found. On top of this, it could also be that TROPOMI observed snow when SCIAMACHY did not (and vice versa). On average, the differences found between the TROPOMI and SCIAMACHY surface LER are rather small.

To provide more quantitative information, we tabulate in Table 3 the results for all months and all wavelengths. Please note that the numbers have been multiplied by 100. Looking at the reported numbers we see that the mean difference is only slightly dependent on the calendar month. No clear seasonal variation can be extracted. The same can be said about the spread (FWHM) of the distribution: it does not depend much on the calendar month. The increase of the spread of the distribution towards shorter wavelengths is presumably a result of the increased difficulty of observing the surface at the shorter wavelengths. The numbers that are found for the spread are in agreement with the spread found earlier comparing the heritage databases [RD5, RD22]. However, it should be noted that the spreads in Table 3 have decreased compared to the previous version (v1.0) of the TROPOMI surface LER database. This is most likely due to a better radiometric calibration and the implementation of degradation correction in the new TROPOMI L1 data.

7.3 Conclusion of the comparison with SCIAMACHY

The main conclusion of the analysis is that the agreement between the TROPOMI and SCIAMACHY surface LER databases is in principle quite good. For the longer wavelength bands (670 to 2314 nm) the TROPOMI surface LER is biased below 0.002 and the requirements (0.02+10% for $\lambda > 600$ nm, see [RD18]) are met easily. For the shorter wavelength bands (328 to 494 nm) the TROPOMI surface LER is biased up to 0.02 and the requirements (0.03+10% for $\lambda < 500$ nm) are met relatively easily as well.

TROPOMI MIN-LER (758 nm) versus SCIAMACHY MIN-LER (758 nm)
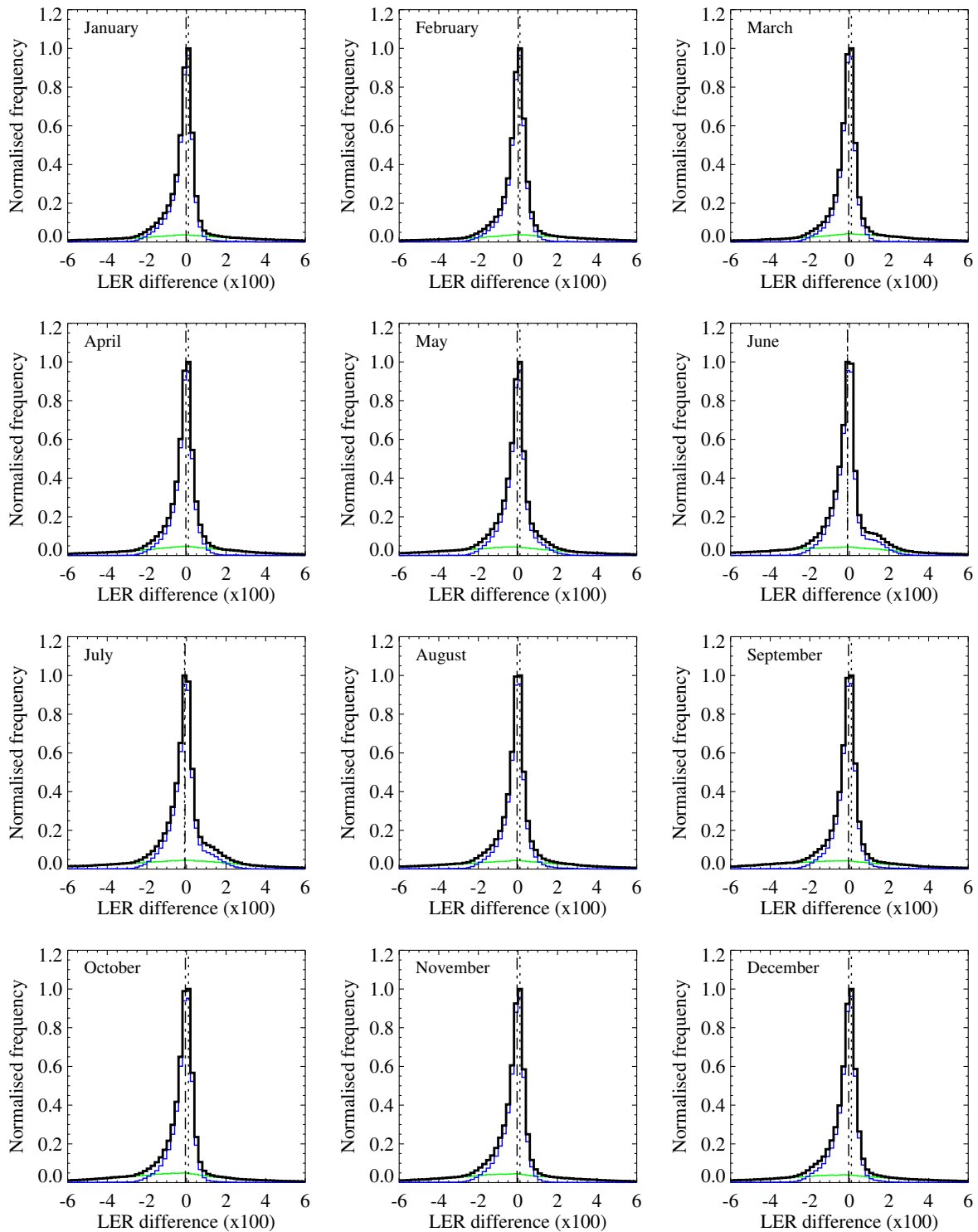
Figure 6: Histogram of the differences in the surface LER databases of TROPOMI and SCIAMACHY at 758 nm. The vertical lines indicate the mean (dashed line) and the mode (dotted line) of the distribution.

TROPOMI MIN-LER (494 nm) versus SCIAMACHY MIN-LER (494 nm)
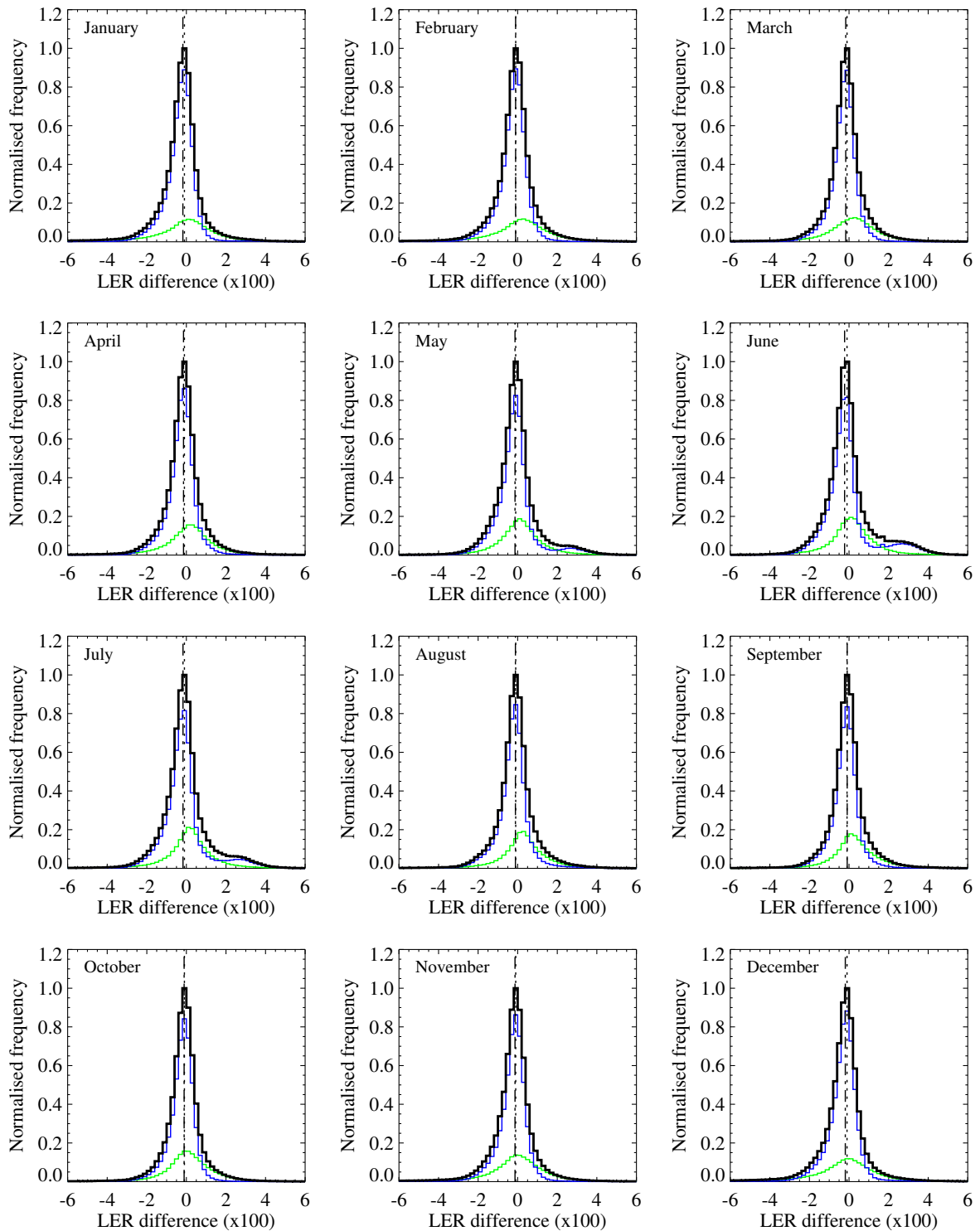
Figure 7: Histogram of the differences in the surface LER databases of TROPOMI and SCIAMACHY at 494 nm. For this wavelength the histograms are somewhat asymmetric, for land and ocean.

TROPOMI MIN-LER (380 nm) versus SCIAMACHY MIN-LER (380 nm)
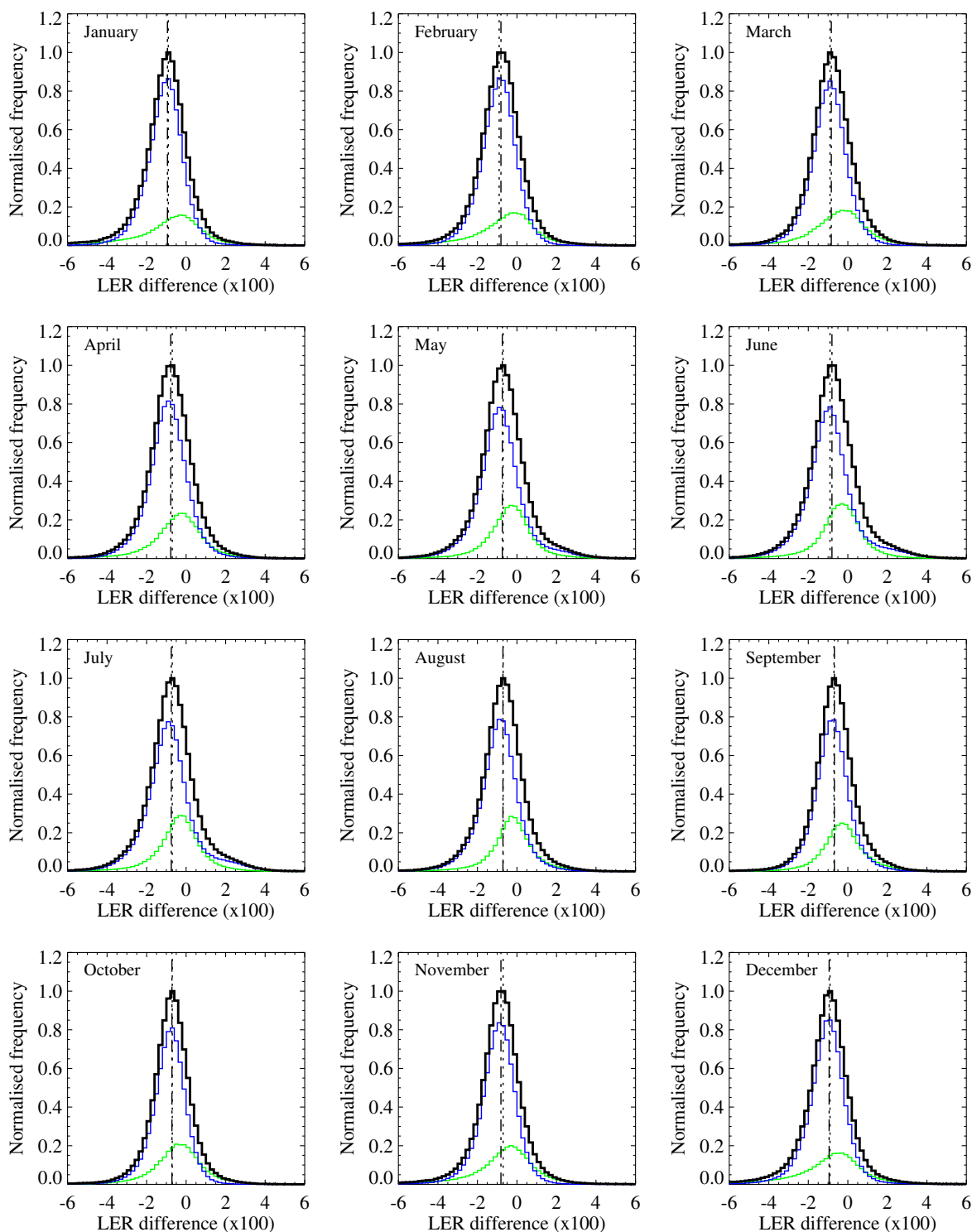
Figure 8: Histogram of the differences in the surface LER databases of TROPOMI and SCIAMACHY at 380 nm. There clearly is a bias of about 0.02 in the TROPOMI surface LER values, for land and ocean.

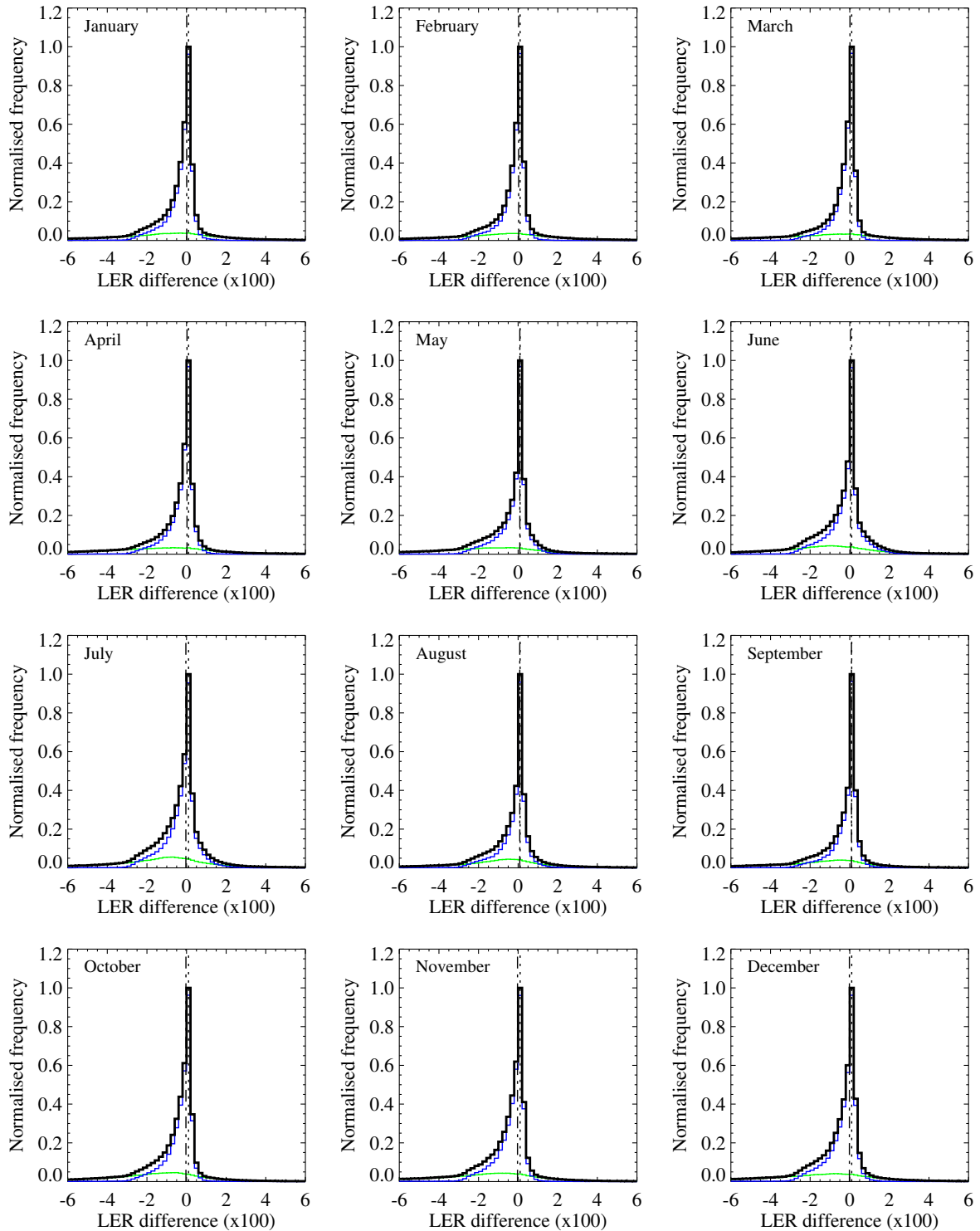**TROPOMI MIN-LER (2314 nm) versus SCIAMACHY MIN-LER (2314 nm)**

Figure 9: Histogram of the differences in the surface LER databases of TROPOMI and SCIAMACHY at 2314 nm. The agreement over ocean is very good. Over land, the histograms are somewhat asymmetric.

TROPOMI versus SCIAMACHY (MIN-LER)											
Mean surface LER difference ($\times 100$)											
λ (nm)	JAN	FEB	MAR	APR	MAY	JUN	JUL	AUG	SEP	OCT	NOV	DEC
328	-2.45	-2.14	-2.14	-2.11	-1.96	-2.02	-1.96	-1.81	-1.74	-1.84	-2.14	-2.45
335	-2.21	-1.94	-1.96	-1.95	-1.83	-1.86	-1.82	-1.73	-1.65	-1.75	-1.98	-2.23
340	-2.58	-2.33	-2.38	-2.38	-2.32	-2.37	-2.31	-2.20	-2.08	-2.19	-2.41	-2.63
354	-2.15	-1.96	-2.01	-1.99	-1.91	-1.98	-1.92	-1.86	-1.78	-1.86	-2.00	-2.16
367	-1.33	-1.17	-1.19	-1.13	-1.05	-1.10	-1.04	-1.03	-1.01	-1.06	-1.18	-1.33
380	-0.94	-0.81	-0.84	-0.78	-0.74	-0.80	-0.75	-0.71	-0.68	-0.72	-0.81	-0.95
388	-0.83	-0.71	-0.74	-0.69	-0.66	-0.72	-0.67	-0.61	-0.59	-0.64	-0.72	-0.85
425	-0.72	-0.61	-0.63	-0.58	-0.54	-0.64	-0.58	-0.51	-0.49	-0.53	-0.60	-0.71
440	-0.56	-0.46	-0.49	-0.46	-0.43	-0.53	-0.48	-0.41	-0.38	-0.41	-0.46	-0.55
463	-0.41	-0.32	-0.37	-0.34	-0.33	-0.43	-0.37	-0.31	-0.28	-0.30	-0.34	-0.41
494	-0.18	-0.11	-0.16	-0.14	-0.14	-0.22	-0.17	-0.12	-0.09	-0.11	-0.14	-0.19
670	0.16	0.20	0.14	0.15	0.14	0.08	0.11	0.14	0.16	0.16	0.16	0.15
685	0.11	0.15	0.10	0.10	0.10	0.04	0.07	0.10	0.11	0.11	0.11	0.11
697	0.08	0.11	0.06	0.06	0.06	0.00	0.03	0.06	0.07	0.06	0.07	0.07
712	0.04	0.08	0.02	0.02	0.02	-0.03	-0.01	0.02	0.02	0.01	0.02	0.02
758	-0.02	0.01	-0.04	-0.03	-0.04	-0.09	-0.07	-0.04	-0.05	-0.05	-0.04	-0.04
772	-0.01	0.02	-0.03	-0.02	-0.02	-0.08	-0.06	-0.03	-0.03	-0.04	-0.03	-0.03
2314	0.01	0.02	0.01	0.02	0.09	0.04	-0.04	0.08	0.09	-0.03	-0.03	-0.02
FWHM of distribution ($\times 100$)											
λ (nm)	JAN	FEB	MAR	APR	MAY	JUN	JUL	AUG	SEP	OCT	NOV	DEC
328	2.76	2.85	2.85	3.11	3.33	3.51	3.40	3.11	2.92	2.65	2.69	2.75
335	2.44	2.48	2.46	2.73	2.97	3.16	3.04	2.70	2.52	2.32	2.39	2.47
340	2.48	2.50	2.51	2.79	2.92	3.05	2.98	2.75	2.54	2.32	2.43	2.49
354	2.41	2.46	2.50	2.77	2.89	3.03	2.98	2.68	2.44	2.25	2.39	2.43
367	2.15	2.21	2.22	2.39	2.49	2.58	2.51	2.25	2.07	1.99	2.10	2.13
380	2.13	2.16	2.15	2.25	2.24	2.32	2.28	2.12	1.98	1.93	2.05	2.08
388	2.05	2.07	2.06	2.14	2.12	2.20	2.16	2.00	1.88	1.84	1.96	2.00
425	1.85	1.83	1.78	1.81	1.76	1.80	1.82	1.75	1.68	1.64	1.77	1.81
440	1.72	1.71	1.66	1.70	1.65	1.67	1.72	1.65	1.57	1.53	1.65	1.69
463	1.51	1.51	1.46	1.52	1.50	1.52	1.57	1.48	1.40	1.38	1.47	1.50
494	1.30	1.30	1.25	1.31	1.34	1.33	1.38	1.28	1.22	1.22	1.29	1.31
670	0.89	0.90	0.86	0.93	0.99	0.98	1.07	0.91	0.90	0.92	0.99	0.97
685	0.87	0.89	0.84	0.91	0.97	0.97	1.05	0.89	0.89	0.91	0.97	0.95
697	0.87	0.88	0.84	0.92	0.99	0.98	1.05	0.89	0.89	0.92	0.98	0.96
712	0.86	0.89	0.84	0.92	1.03	1.02	1.08	0.90	0.92	0.93	0.98	0.96
758	0.82	0.86	0.81	0.89	0.96	0.95	1.00	0.85	0.86	0.88	0.92	0.91
772	0.81	0.85	0.80	0.88	0.94	0.94	0.98	0.84	0.85	0.87	0.90	0.90
2314	0.69	0.64	0.63	0.65	0.47	0.67	1.01	0.48	0.45	0.77	0.83	0.83

Table 3: Mean difference in the surface LER of the TROPOMI and SCIAMACHY surface LER databases. The FWHM of the distribution is also given. The numbers have been multiplied by 100.

8 TROPOMI versus OMI

In this section, we compare the TROPOMI surface LER database with the OMI surface LER database. Because of the orbital and instrumental similarities between TROPOMI and OMI, the OMI surface LER database should, at least on paper, be the ideal reference. Unfortunately, because of the limited spectral range of the OMI instrument, only the wavelength bands ranging from 328 to 494 nm can be compared in this study.

8.1 Global maps of the differences

In Figure 10 we present the difference between the 494-nm surface LER from the TROPOMI and OMI surface LER databases for the month March. The agreement is in general rather good. Over the ocean the differences are very close to zero. Mild blue features are also seen, in the ocean close to Antarctica, which could point to less cloud contamination in the TROPOMI surface LER database. It may also be a result of the different retrieval approach in the presence of sea ice. Over land the differences are close to zero for most non-snow/ice surfaces. Especially over Europe and Australia agreement is very good. We find small positive differences for parts of South America and for the northern part of the African continent.

In Figure 11 we present the global map of the differences between TROPOMI and OMI for 380 nm, again for the month March. There is again good agreement over the ocean, although there is some blue in the plot. Over land the agreement is very good for most of the land. An exception is the area in the northern part of South America. There are clearly some (mild) red patches here. A red colour could point to cloud contamination in the TROPOMI surface LER database. However, this is not expected because the TROPOMI surface LER database is based on much more data than the OMI surface LER database. Also, cloud contamination would then have shown up in Figure 10 and this did not happen.

8.2 Statistical analysis of the differences

We calculate the distributions of the differences for each month of the year, for each of the OMI surface LER wavelength bands that coincide with the TROPOMI surface LER wavelength bands (see Table 2). In Figures 12 and 13 we present the results. As can be seen, the histograms for 494 nm are not very symmetric but do have their mean and mode values close to zero. This is the case for all months of the year. So, for 494 nm the agreement is good. For 380 nm the distributions are more symmetric and the bias is also very close to zero for all calendar months and for both land and ocean surfaces.

In Table 4 we present the numerical results of the histogram analyses. The table presents the mean surface LER difference for each month of the year and for each of the wavelength bands that could be compared. It also lists the spread (FWHM) of the distribution. All numbers were multiplied by 100. Note that especially for the wavelength bands above 380 nm the agreement is very good. Also notice that the spread of the difference distribution at 494 nm (January: 0.013) is the same as that found for the TROPOMI versus SCIAMACHY surface LER comparison (see Table 3). But at 328 nm the spread for the comparison with OMI (January: 0.0189) is smaller than for the comparison with SCIAMACHY (January: 0.0276). That is, the OMI surface LER database is probably a more accurate reference to compare the TROPOMI surface LER database with. We conclude that the TROPOMI and OMI surface LER products are in very good agreement.

8.3 Conclusion of the comparison with OMI

The comparison with the OMI surface LER product indicates that the TROPOMI surface LER product is of good quality. Deviations are found, but these are in general small over the ocean and over most of the land. For all wavelength bands, the systematic (negative) bias that is found is on the order of 0.006–0.018. The requirements (0.03+10% for $\lambda < 500$ nm, see [RD18]) are therefore met relatively easily.

TROPOMI (494 nm) − OMI (494 nm)

MIN-LER

MARCH

-0.08   -0.06   -0.04   -0.02   0.00   0.02   0.04   0.06   0.08
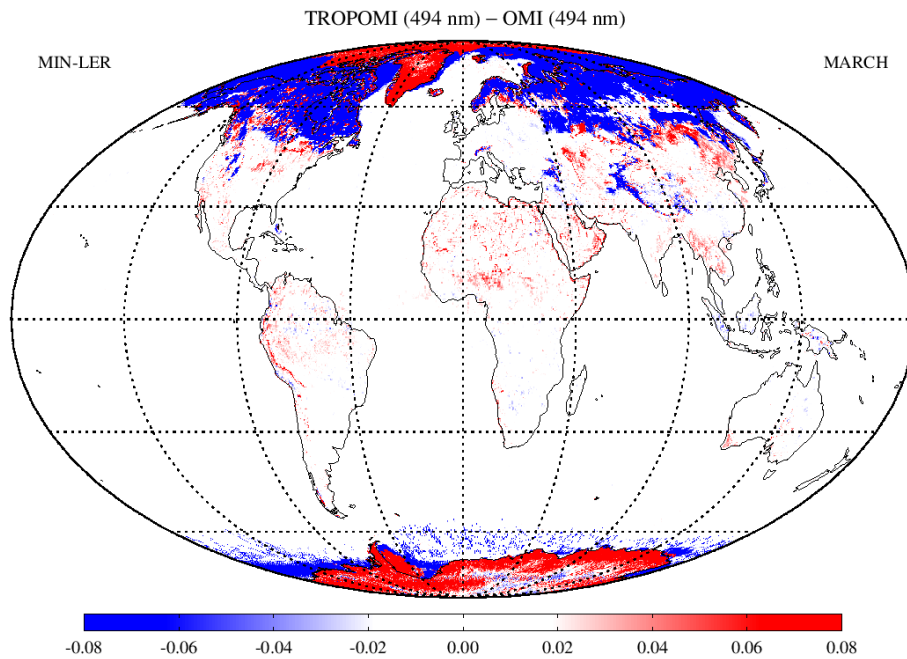
Figure 10: Map of the difference between the 494-nm surface LER from the TROPOMI and OMI surface LER databases, for the month March. Over the ocean the agreement is very good. Over land the agreement is good for most areas.

TROPOMI (380 nm) − OMI (380 nm)

MIN-LER

MARCH

-0.08   -0.06   -0.04   -0.02   0.00   0.02   0.04   0.06   0.08
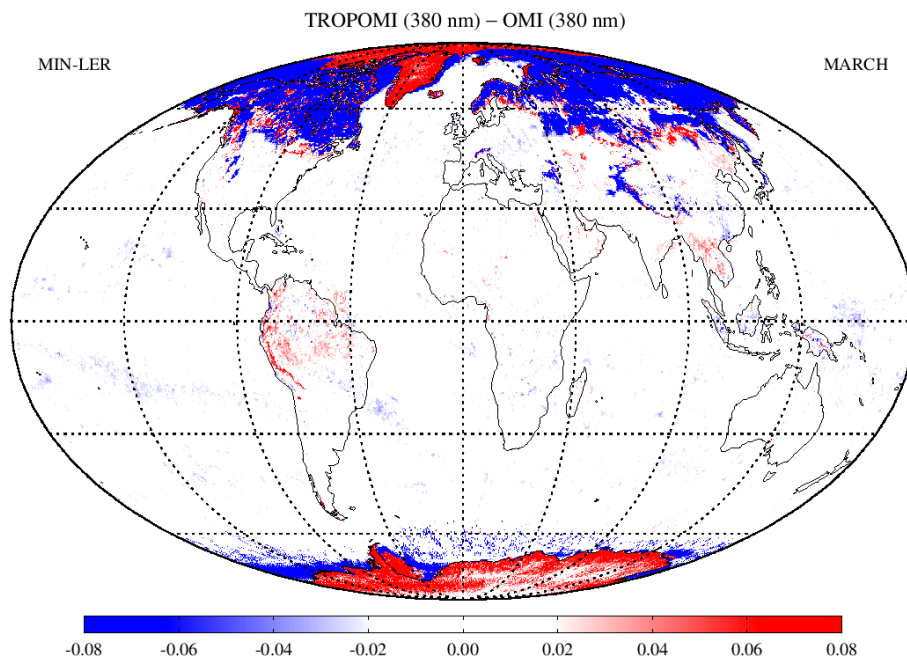
Figure 11: Map of the difference between the 380-nm surface LER from the TROPOMI and OMI surface LER databases, for the month March. The agreement over the ocean is good, although some blue is present in the plot. Over land, agreement is good everywhere, with only some red in the Amazonian region.

European Space Agency
Agence spatiale européenne

TROPOMI MIN-LER (494 nm) versus OMI MIN-LER (494 nm)
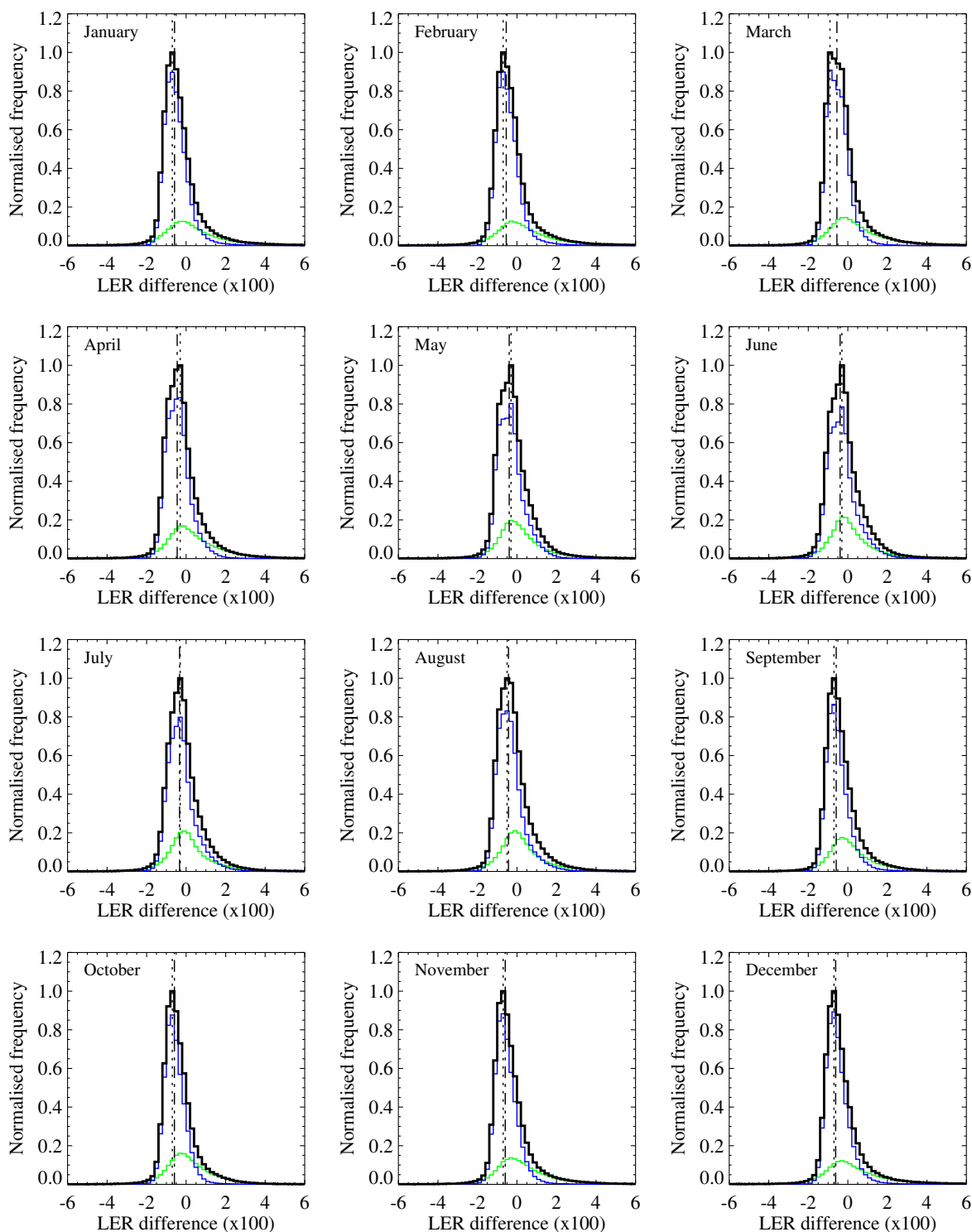
Figure 12: Histogram of the differences in the surface LER databases of TROPOMI and OMI at 494 nm. The colour blue is used for water, green is used for land. The agreement is good for all calendar months.

TROPOMI MIN-LER (380 nm) versus OMI MIN-LER (380 nm)
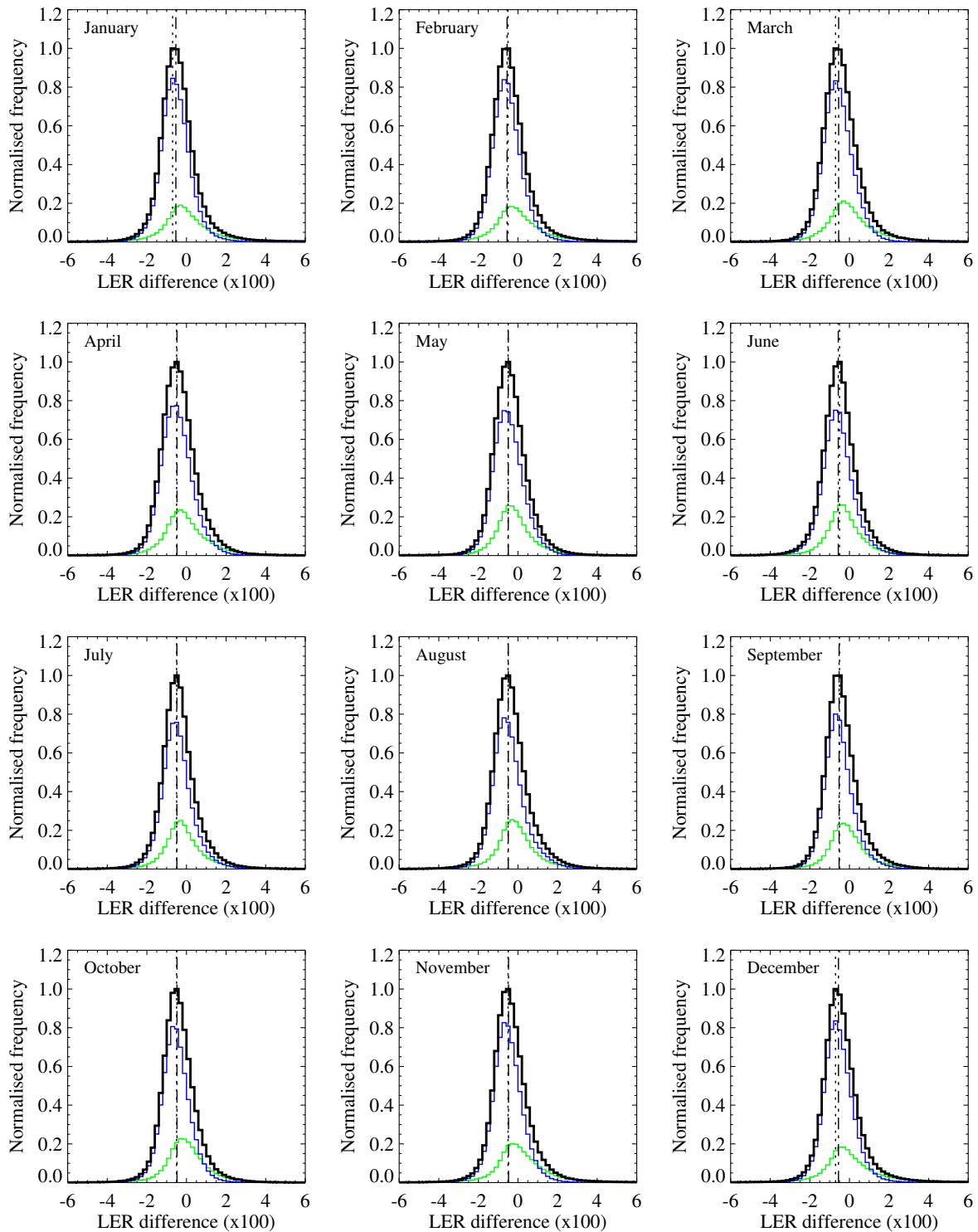
Figure 13: Histogram of the differences in the surface LER databases of TROPOMI and OMI at 380 nm. The colour blue is used for water, green is used for land. The agreement is good for all calendar months.

TROPOMI versus OMI (MIN-LER)											
Mean surface LER difference ($\times$100)											
λ (nm)	JAN	FEB	MAR	APR	MAY	JUN	JUL	AUG	SEP	OCT	NOV	DEC
328	-1.20	-1.31	-1.27	-1.22	-1.19	-1.27	-1.16	-1.10	-1.04	-0.90	-0.91	-1.11
335	-1.31	-1.36	-1.36	-1.36	-1.41	-1.52	-1.42	-1.37	-1.26	-1.13	-1.09	-1.25
342	-1.82	-1.85	-1.87	-1.89	-1.95	-2.08	-1.97	-1.91	-1.80	-1.66	-1.63	-1.78
354	-1.31	-1.33	-1.35	-1.35	-1.41	-1.53	-1.42	-1.35	-1.28	-1.15	-1.12	-1.27
367	-0.96	-0.98	-0.98	-0.96	-1.02	-1.14	-1.05	-0.97	-0.94	-0.86	-0.86	-0.97
380	-0.53	-0.55	-0.55	-0.48	-0.49	-0.56	-0.48	-0.49	-0.52	-0.48	-0.48	-0.55
388	-0.89	-0.89	-0.89	-0.83	-0.84	-0.92	-0.83	-0.82	-0.86	-0.83	-0.83	-0.92
416	-1.00	-0.96	-0.94	-0.86	-0.86	-0.93	-0.84	-0.86	-0.96	-0.95	-0.97	-1.04
425	-0.93	-0.89	-0.87	-0.78	-0.75	-0.81	-0.72	-0.77	-0.89	-0.89	-0.91	-0.97
440	-0.83	-0.79	-0.78	-0.68	-0.64	-0.68	-0.60	-0.67	-0.80	-0.79	-0.81	-0.86
463	-0.77	-0.72	-0.72	-0.62	-0.56	-0.58	-0.51	-0.60	-0.75	-0.76	-0.77	-0.80
494	-0.59	-0.54	-0.55	-0.45	-0.39	-0.39	-0.33	-0.43	-0.59	-0.59	-0.59	-0.61
FWHM of distribution ($\times$100)											
λ (nm)	JAN	FEB	MAR	APR	MAY	JUN	JUL	AUG	SEP	OCT	NOV	DEC
328	1.89	1.94	1.94	1.93	1.85	1.92	1.85	1.91	1.78	1.84	1.92	1.84
335	1.81	1.83	1.84	1.83	1.80	1.82	1.76	1.83	1.75	1.79	1.83	1.79
342	1.83	1.84	1.88	1.92	1.92	1.93	1.86	1.88	1.76	1.79	1.82	1.79
354	1.82	1.87	1.90	1.93	1.90	1.89	1.82	1.84	1.74	1.77	1.79	1.79
367	1.74	1.76	1.82	1.83	1.76	1.76	1.70	1.79	1.65	1.67	1.71	1.71
380	1.68	1.71	1.78	1.83	1.73	1.69	1.64	1.74	1.62	1.65	1.70	1.67
388	1.68	1.72	1.79	1.82	1.72	1.69	1.63	1.73	1.63	1.67	1.72	1.67
416	1.58	1.62	1.68	1.72	1.64	1.63	1.56	1.65	1.56	1.61	1.65	1.59
425	1.54	1.57	1.63	1.69	1.63	1.61	1.55	1.62	1.51	1.55	1.61	1.54
440	1.47	1.49	1.55	1.63	1.59	1.59	1.53	1.57	1.45	1.47	1.52	1.46
463	1.34	1.36	1.41	1.51	1.52	1.54	1.48	1.48	1.34	1.33	1.36	1.32
494	1.30	1.28	1.31	1.42	1.45	1.50	1.44	1.42	1.26	1.23	1.25	1.24

**Table 4**: Mean difference in the surface LER of the TROPOMI and OMI surface LER databases. The FWHM of the distribution is also given. The numbers have been multiplied by 100.

European Space Agency
Agence spatiale européenne

9 TROPOMI versus GOME-2

In this section, we compare the TROPOMI surface LER product with the GOME-2 surface LER product. The GOME-2 surface LER database provides a reliable reference for all wavelength bands in the TROPOMI surface LER database, except for the wavelength band at 2314 nm. The overpass times at the equator are different (TROPOMI: 13:30 LT; GOME-2: 09:30 LT). This can cause differences because of surface BRDF effects.

9.1 Global maps of the differences

In Figure 14 we plot the difference between the TROPOMI and GOME-2 surface LER for the 758-nm wavelength band for the month March. Over the ocean, the differences are very small and mild features are seen which were already seen before when the TROPOMI surface LER database was compared to the SCIAMACHY surface LER database (see Figure 2). Over land, positive and negative biases are found. It is best to compare Figure 14 with Figure 2. The similarity between these two figures is large. This could have been expected, because the SCIAMACHY and GOME-2 surface LER databases were found to agree well [RD5]. On the other hand, it does indicate that the TROPOMI surface LER is the reason for the differences that are found.

Figure 15 presents the results for the 494-nm wavelength band. Here the agreement over ocean and (snow-free) land is rather good. It makes sense to compare the map with the maps shown in Figures 3 and 10. There is a clear similarity between the three images. Especially the similarity with the TROPOMI–SCIAMACHY intercomparison is striking. But there also is a clear similarity with the TROPOMI–OMI intercomparison. This holds for ocean, land, and snow/ice surfaces. The conclusion is straightforward: the SCIAMACHY, OMI, and GOME-2 surface LER database agree with each other in such a way that we can safely attribute the small deviations that are found to the TROPOMI surface LER database. However, this does not mean that the TROPOMI surface LER database does a worse job. In fact, the many improvements of the TROPOMI surface LER database w.r.t. the heritage LER databases are bound to produce deviations.

In Figure 16 we present the differences between the TROPOMI and GOME-2 surface LER databases for the 380-nm wavelength band for the month March. This time the agreement is not very good. There is a clear negative bias, mostly over the ocean, but to a lesser degree also partly over land. The bad agreement is almost completely explained by a 0.01–0.02 bias in the GOME-2 surface LER database for wavelengths below 400 nm [RD5]. This positive bias in the GOME-2 surface LER database needs to be taken into account when interpreting the results. When we do this, we see again a striking similarity with the TROPOMI–SCIAMACHY and TROPOMI–OMI results (see Figures 4 and 11).

9.2 Statistical analysis of the differences

Statistical analyses of the differences between the TROPOMI and GOME-2 surface LER databases are presented in Figures 17 to 19 in the form of histograms of the surface LER differences that were found. As before, we only consider surface LER data with latitudes between 60°N and 60°S. Black histograms represent all possible scenes, the blue histograms are based on scenes over water, the green histograms are based on scenes over land and/or snow/ice. The mean of the distribution is represented by the dashed vertical line, the mode of the distribution is given by the dotted vertical line.

Figure 17 presents the result for the 758-nm wavelength band. The results indicate that there is a good agreement between the TROPOMI an GOME-2 surface LER database at this wavelength. The distributions are reasonably symmetric, and the mean biases are close to zero. This is the case for all calendar months. The histograms are also very much in agreement with the histograms that were presented in Figure 6. Next, in Figure 18 the results for the 494-nm wavelength band are presented. The histograms are slightly asymmetric, which was also the case for the TROPOMI–SCIAMACHY comparison (see section 7.2). In fact, there is a very good agreement between Figure 18 and Figure 7. As explained in section 9.1, this could have been expected, because the SCIAMACHY and GOME-2 surface LER databases were found to agree well [RD5].

Finally, in Figure 19 we present the histograms for the 380-nm wavelength band. Minor differences between land and ocean are found, in agreement with what was reported in section 9.1 for this wavelength. The bias in the LER difference is negative with a magnitude of about 0.01–0.02, depending mainly on the surface type (land/ocean) and also somewhat on the calendar month. Note that, as explained in section 9.1, the biases can be explained by the fact that the GOME-2 surface LER is biased by about 0.01–0.02 for wavelengths below 400 nm [RD5]. Taking this bias into account we find that there is a good quantitative and qualitative agreement between with the histograms presented earlier in Figures 8 and 13.

More quantitative information is tabulated in Table 5, which presents the results for all months and all wavelengths. Please note that the numbers have been multiplied by 100. Looking at the reported numbers we

TROPOMI (758 nm) – GOME-2ABC (758 nm)

Figure 14: Map of the difference between the 758-nm surface LER from the TROPOMI and GOME-2 surface LER databases. Over the ocean, the agreement is good. Over land, positive and negative biases are found, depending on the location. There is quite some similarity with the results presented in Figure 2.

TROPOMI (494 nm) – GOME-2ABC (494 nm)

Figure 15: Map of the difference between the 494-nm surface LER from the TROPOMI and GOME-2 surface LER databases. Over land and ocean the agreement is good. Compare with Figures 3 and 10. The blue haze near latitudes of 50°S may be related to mild cloud contamination in the GOME-2 surface LER database.

TROPOMI (380 nm) – GOME-2ABC (380 nm)

MIN-LER

MARCH
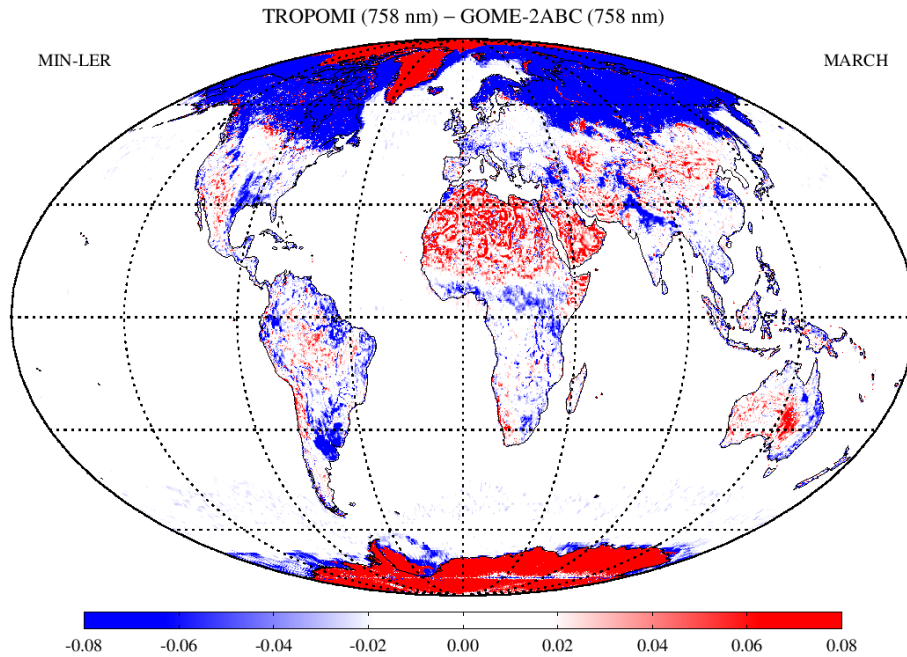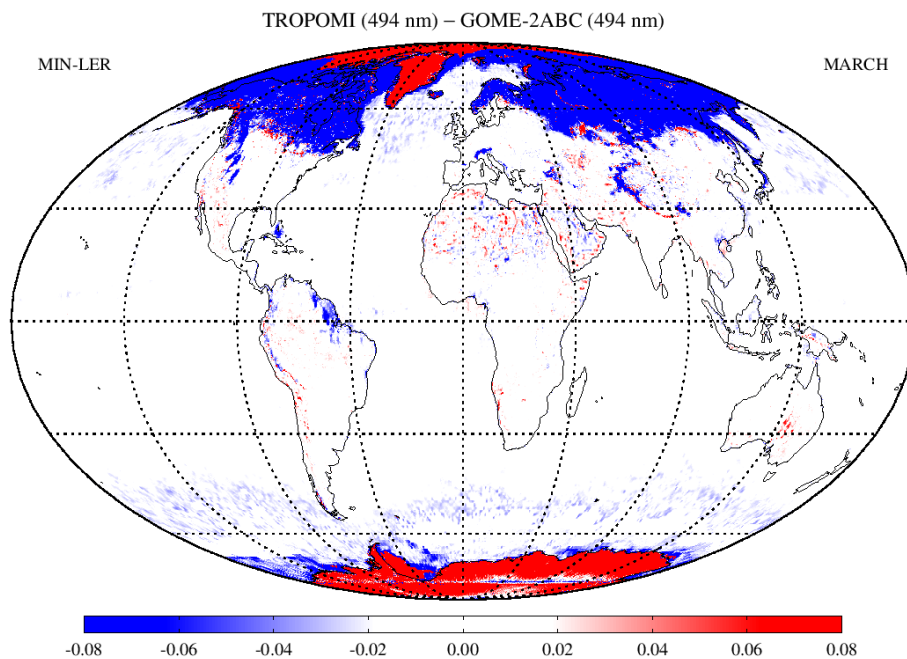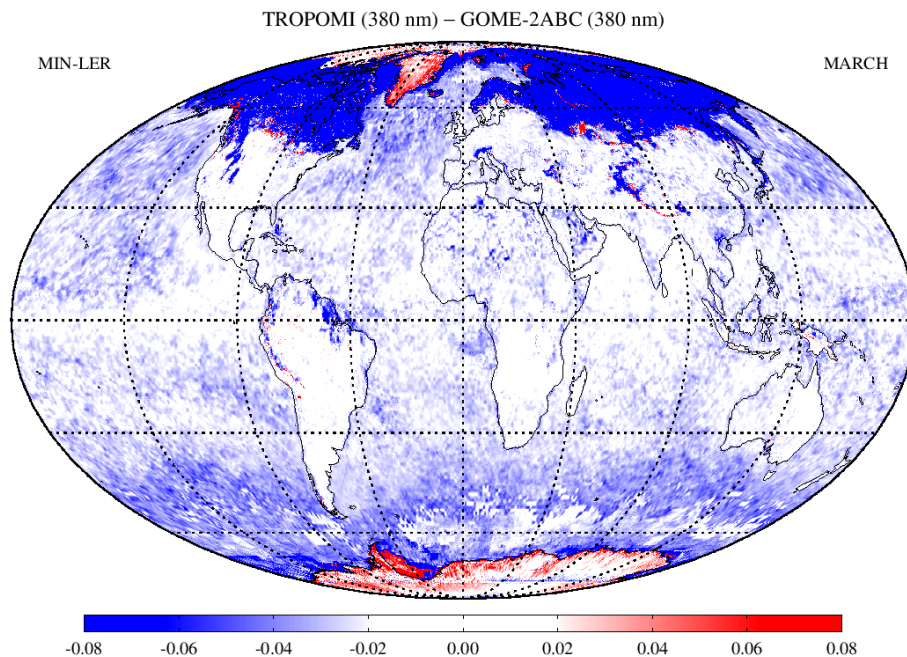

-0.08   -0.06   -0.04   -0.02   0.00   0.02   0.04   0.06   0.08

Figure 16: Map of the difference between the 380-nm surface LER from the TROPOMI and GOME-2 surface LER databases. The negative bias, caused by the GOME-2 surface LER database, is evident.

see that the mean difference is only slightly dependent on the calendar month. No clear seasonal variation can be extracted. The same can be said about the spread (FWHM) of the distribution: it does not depend much on the calendar month. The increase of the spread of the distribution towards shorter wavelengths is presumably a result of the increased difficulty of observing the surface at the shorter wavelengths. The numbers that are found for the spread are in agreement with the spread found earlier comparing the heritage databases [RD5, RD22]. However, it is important to note that the spread has gone down considerably compared to the spread found using the previous version (v1.0) of the TROPOMI surface LER database. This is related to improvements of the radiometric calibration and the introduction of a degradation correction in the TROPOMI collection-3 L1 product. The decrease in the spread is a clear sign of improvement of the quality.

When we compare the numbers in Table 5 to the numbers found in the TROPOMI–SCIAMACHY comparison (see Table 3) we observe a very good agreement for wavelengths above 400 nm. Below 400 nm there is a $\sim$0.03 difference here which is partly explained by the bias of 0.01–0.02 in the GOME-2 surface LER database for wavelengths below 400 nm [RD5]. This bias has to be taken into account when interpreting the numbers.

9.3   Conclusion of the comparison with GOME-2

The comparison between the TROPOMI and GOME-2 surface LER database shows striking similarities with the TROPOMI–SCIAMACHY and TROPOMI–OMI surface LER comparisons. For the longer wavelength bands (416 to 772 nm) the TROPOMI surface LER is biased by less than 0.01 and the requirements (0.03+10% for $\lambda < 500$ nm and 0.02+10% for $\lambda > 600$ nm, see [RD18]) are met easily. For the shorter wavelength bands (328 to 388 nm) the biases that are found have magnitudes 0.02–0.05, but these are attributed to (reported) biases in the GOME-2 surface LER database for wavelength bands below 400 nm.

TROPOMI MIN-LER (758 nm) versus GOME-2ABC MIN-LER (758 nm)
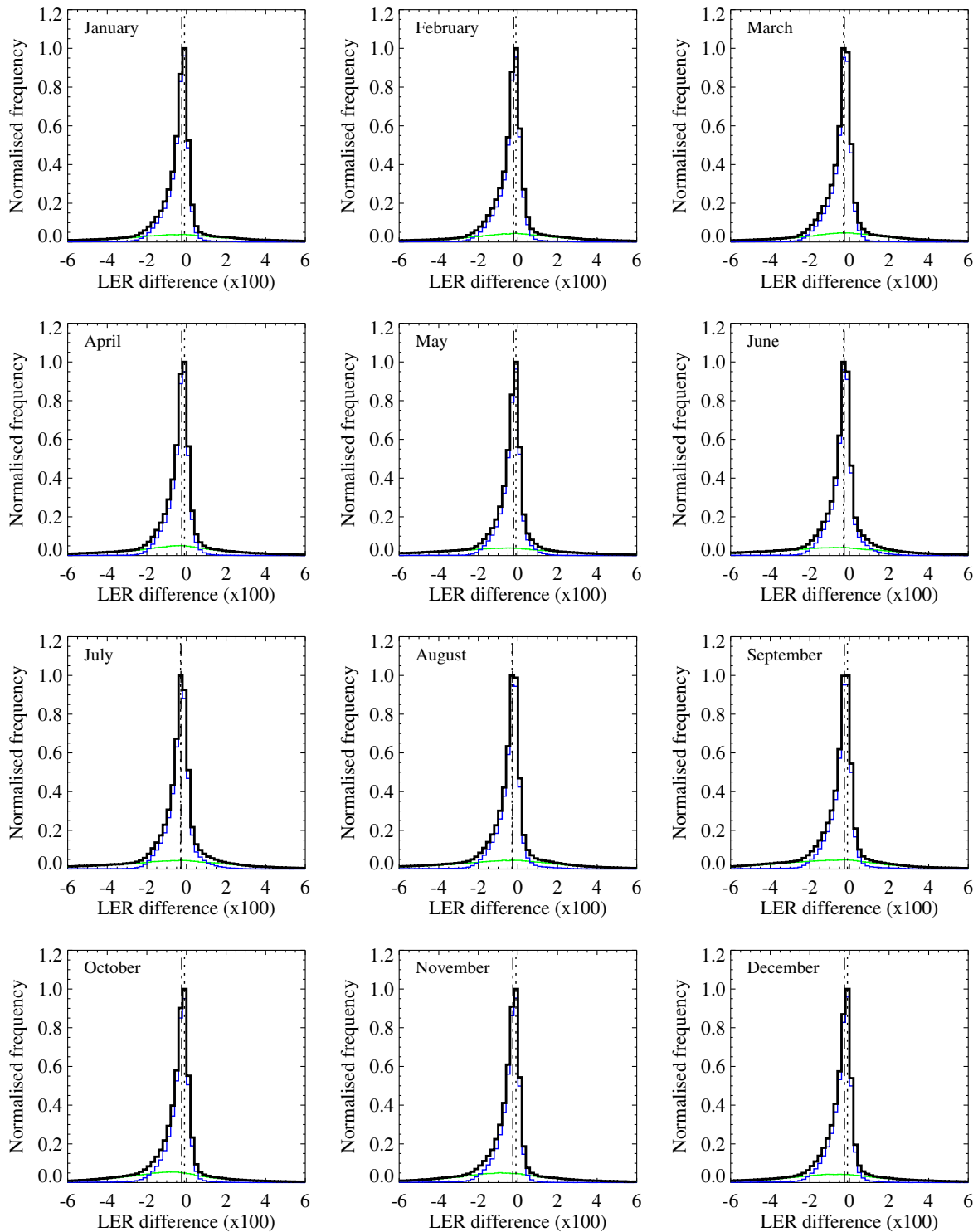
Figure 17: Histogram of the differences in the surface LER databases of TROPOMI and GOME-2 at 758 nm. The histograms do not show a clear bias. A clear dependence on the calendar month is also not found.

TROPOMI MIN-LER (494 nm) versus GOME-2ABC MIN-LER (494 nm)
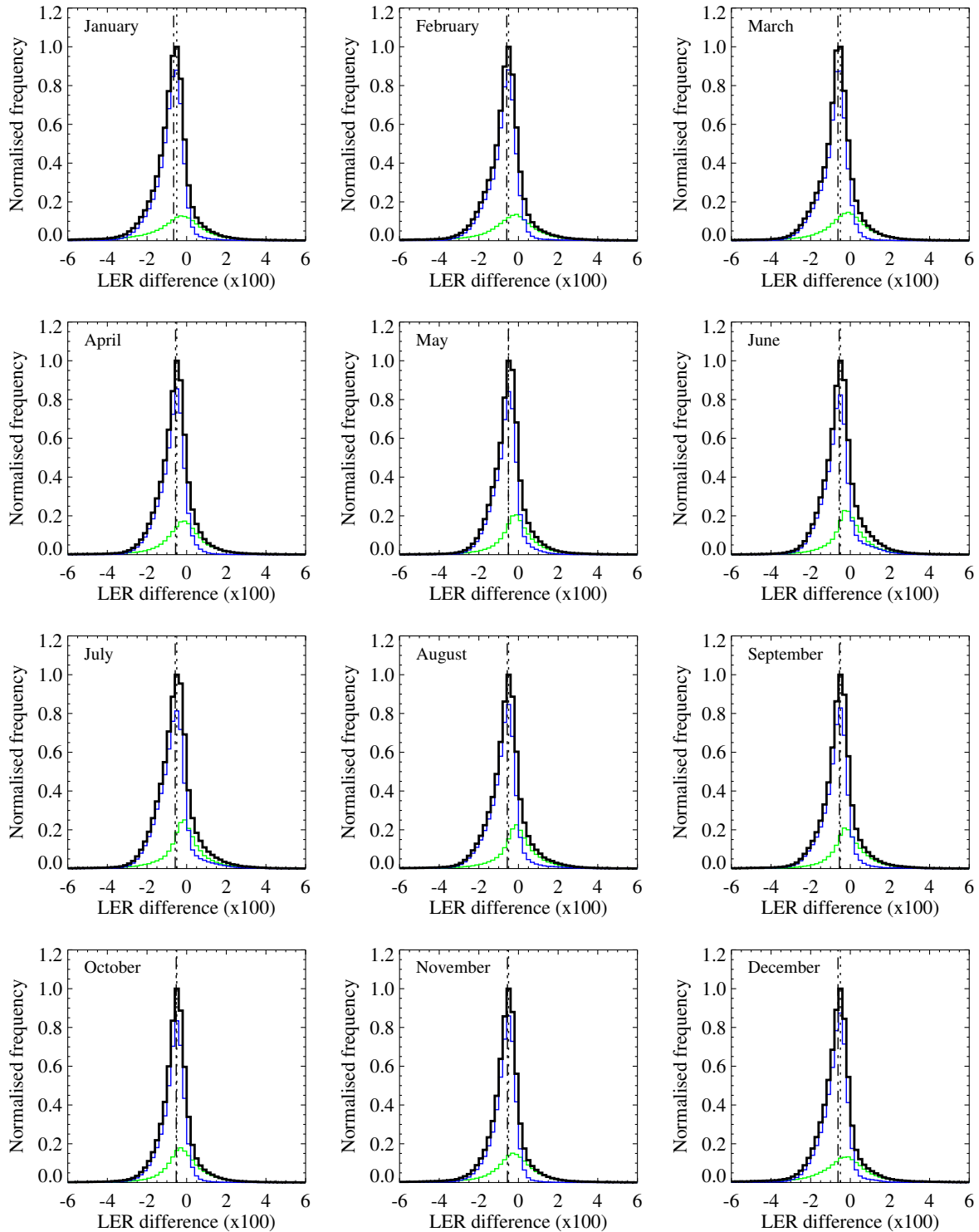
Figure 18: Histogram of the differences in the surface LER databases of TROPOMI and GOME-2 at 494 nm. The histograms are symmetric and no clear difference in behaviour between land and ocean can be seen.

TROPOMI MIN-LER (380 nm) versus GOME-2ABC MIN-LER (380 nm)

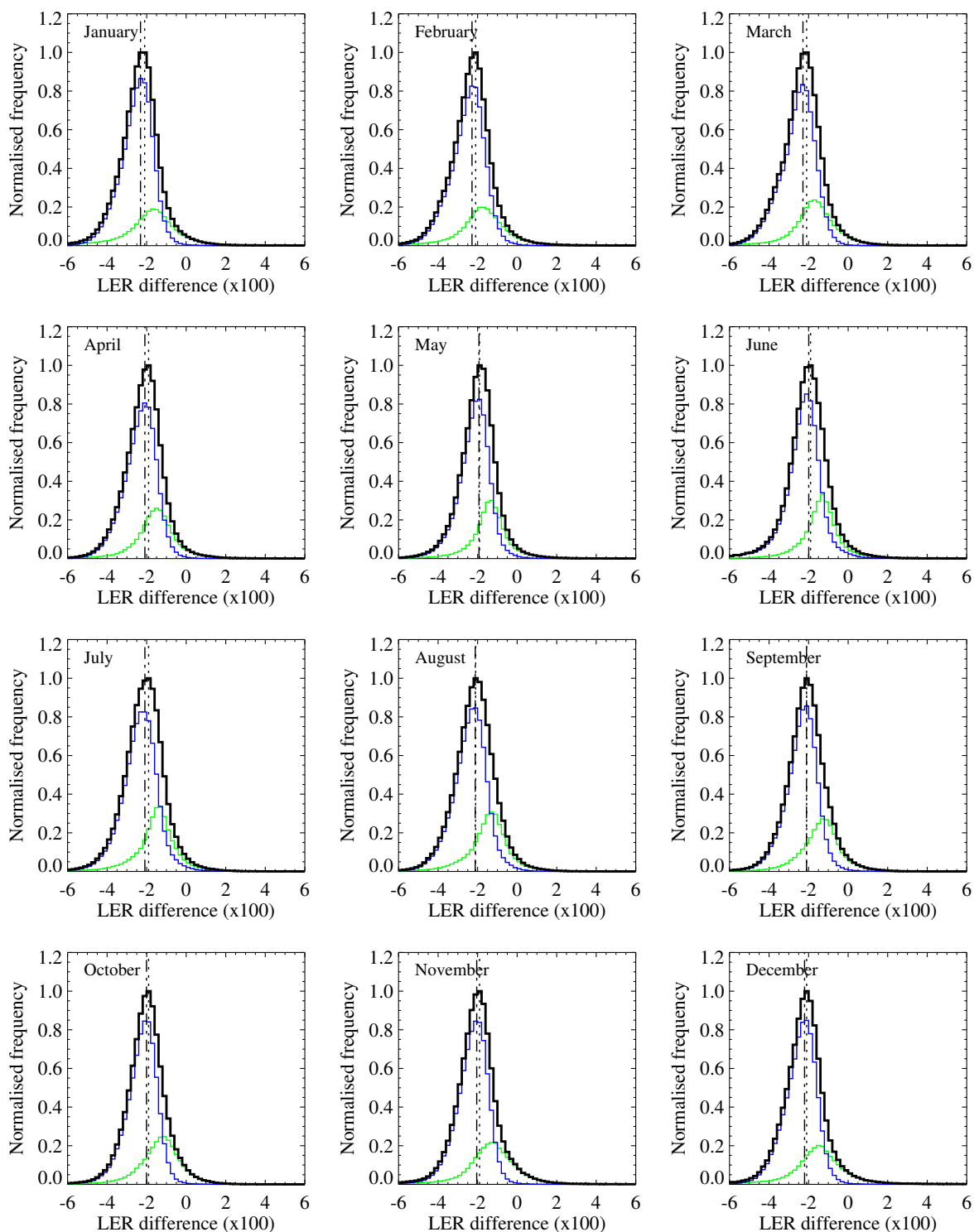**Figure 19**: Histogram of the differences in the surface LER databases of TROPOMI and GOME-2 at 380 nm. There is a relatively large negative bias present of about 0.01–0.02. Also compare with Figures 8 and 13.

TROPOMI versus GOME-2ABC (MIN-LER)											
Mean surface LER difference ($\times 100$)											
λ (nm)	JAN	FEB	MAR	APR	MAY	JUN	JUL	AUG	SEP	OCT	NOV	DEC
328	-5.27	-5.20	-4.97	-4.31	-3.75	-3.76	-4.02	-4.32	-4.44	-4.51	-4.64	-4.99
335	-4.26	-4.21	-4.09	-3.56	-3.18	-3.19	-3.38	-3.56	-3.67	-3.71	-3.77	-4.07
340	-4.13	-4.10	-4.03	-3.59	-3.25	-3.26	-3.44	-3.60	-3.69	-3.69	-3.75	-3.99
354	-3.45	-3.42	-3.36	-3.03	-2.77	-2.80	-2.95	-3.05	-3.08	-3.03	-3.09	-3.30
367	-2.67	-2.65	-2.61	-2.37	-2.16	-2.20	-2.32	-2.39	-2.41	-2.34	-2.39	-2.56
380	-2.31	-2.28	-2.28	-2.09	-1.93	-1.99	-2.09	-2.12	-2.11	-2.01	-2.05	-2.20
388	-2.26	-2.22	-2.24	-2.06	-1.94	-2.00	-2.07	-2.07	-2.06	-1.97	-2.02	-2.17
416	-1.39	-1.32	-1.32	-1.16	-1.07	-1.13	-1.18	-1.15	-1.17	-1.14	-1.19	-1.32
425	-1.31	-1.24	-1.23	-1.10	-0.99	-1.05	-1.10	-1.10	-1.11	-1.07	-1.12	-1.23
440	-1.09	-1.02	-1.04	-0.91	-0.83	-0.89	-0.92	-0.92	-0.92	-0.88	-0.93	-1.02
463	-0.97	-0.89	-0.91	-0.81	-0.75	-0.80	-0.83	-0.82	-0.81	-0.79	-0.82	-0.91
494	-0.66	-0.59	-0.62	-0.56	-0.51	-0.56	-0.58	-0.57	-0.55	-0.53	-0.56	-0.62
670	-0.14	-0.11	-0.15	-0.13	-0.10	-0.15	-0.17	-0.16	-0.13	-0.10	-0.12	-0.14
685	-0.15	-0.13	-0.17	-0.14	-0.12	-0.17	-0.19	-0.18	-0.15	-0.12	-0.14	-0.16
697	-0.19	-0.16	-0.20	-0.18	-0.16	-0.21	-0.22	-0.21	-0.18	-0.16	-0.18	-0.19
712	-0.21	-0.18	-0.22	-0.20	-0.18	-0.22	-0.24	-0.23	-0.21	-0.20	-0.21	-0.22
747	-0.25	-0.23	-0.27	-0.25	-0.23	-0.28	-0.29	-0.28	-0.26	-0.25	-0.27	-0.26
758	-0.23	-0.22	-0.26	-0.24	-0.22	-0.27	-0.28	-0.27	-0.26	-0.24	-0.26	-0.25
772	-0.25	-0.24	-0.27	-0.25	-0.24	-0.28	-0.30	-0.29	-0.27	-0.26	-0.28	-0.27
FWHM of distribution ($\times 100$)											
λ (nm)	JAN	FEB	MAR	APR	MAY	JUN	JUL	AUG	SEP	OCT	NOV	DEC
328	2.40	2.29	2.28	2.34	2.61	2.71	2.64	2.57	2.46	2.22	2.44	2.45
335	2.10	2.01	1.99	1.97	2.15	2.34	2.30	2.22	2.09	1.93	2.11	2.15
340	2.00	1.95	1.93	1.82	1.93	2.13	2.12	2.02	1.95	1.86	2.04	2.07
354	2.00	2.00	2.00	1.82	1.77	1.92	1.98	1.97	1.94	1.92	2.01	2.04
367	1.90	1.94	1.94	1.78	1.65	1.77	1.88	1.91	1.87	1.86	1.91	1.94
380	1.96	2.00	2.03	1.94	1.79	1.92	2.08	2.11	1.99	1.91	1.92	1.95
388	1.91	1.96	1.96	1.89	1.76	1.88	2.02	2.02	1.91	1.84	1.85	1.91
416	1.71	1.74	1.74	1.65	1.48	1.58	1.73	1.68	1.54	1.48	1.52	1.65
425	1.71	1.74	1.72	1.64	1.48	1.58	1.72	1.68	1.52	1.46	1.50	1.65
440	1.65	1.66	1.65	1.59	1.45	1.56	1.69	1.63	1.46	1.39	1.43	1.59
463	1.53	1.54	1.51	1.49	1.40	1.51	1.63	1.53	1.36	1.30	1.33	1.48
494	1.35	1.37	1.33	1.36	1.29	1.40	1.49	1.37	1.24	1.17	1.17	1.32
670	0.85	0.89	0.81	0.87	0.85	0.89	1.01	0.85	0.84	0.86	0.85	0.89
685	0.83	0.87	0.80	0.85	0.83	0.87	0.98	0.83	0.83	0.85	0.84	0.88
697	0.83	0.87	0.81	0.85	0.84	0.86	0.96	0.83	0.84	0.86	0.85	0.88
712	0.83	0.88	0.82	0.87	0.87	0.89	0.97	0.86	0.87	0.89	0.87	0.90
747	0.84	0.91	0.86	0.88	0.87	0.88	0.95	0.86	0.87	0.89	0.88	0.91
758	0.83	0.90	0.85	0.88	0.85	0.86	0.92	0.85	0.87	0.89	0.87	0.90
772	0.83	0.90	0.85	0.87	0.86	0.86	0.93	0.85	0.87	0.89	0.88	0.91

Table 5: Mean difference in the surface LER of the TROPOMI and GOME-2ABC surface LER databases. The FWHM of the distribution is also given. The numbers have been multiplied by 100.

European Space Agency
Agence spatiale européenne

10 TROPOMI DLER versus MODIS BRDF

In this section we compare the TROPOMI surface DLER database with MODIS surface BRDF data. The DLER product is by definition a Lambertian product, meaning that it will describe surface reflection optimally when it is used in a radiative transfer model that includes Lambertian surface reflection. The MODIS BRDF product, on the other hand, has to be used when the radiative transfer model can handle surface BRDF. Surface DLER and BRDF by definition are different properties, as shown in section 7 of the ATBD [RD16].

Because DLER and BRDF are fundamentally different properties, we cannot compare the two *and* expect to find a perfect agreement between the two. For the UV wavelength range, where the Rayleigh optical thickness is high, we will have substantial multiple scattering. In these circumstances there will be quite some light paths which visit the surface more than once. In these cases, the (directional) Lambertian model cannot be expected to agree with the BRDF. But, for the longest wavelengths most light paths are only scattered once (and only at the surface). In such cases the DLER and BRDF should be much more alike. This is described extensively in section 7 of the ATBD [RD16]. We will compare the two databases for a number of surface type regions.

10.1 Surface anisotropy

Before presenting the validation approach and the validation results, we first study the magnitude of the surface anisotropy recorded in the TROPOMI surface DLER database. To do this, we define the anisotropy parameter as the DLER at a viewing angle of $-45°$ ("east viewing direction") minus the DLER at viewing angle $+45°$ ("west viewing direction"). For the TROPOMI orbit this parameter is a good indicator for the magnitude and range of the surface anisotropy in the TROPOMI orbit swath. In the left column of Figure 20 this parameter is plotted for the month March, for the wavelength bands at 772, 670, and 463 nm. Alternatively, in the right column of Figure 20 the surface anisotropy is presented as a percentage of the (non-directional) TROPOMI LER.

At 772 nm the surface anisotropy can be as large as 0.16 for vegetated areas. For the typical desert areas the differences are much smaller (0.04–0.08) because non-vegetated surfaces are usually more isotropic than vegetated areas. The values over the vegetated areas correspond to percentages of 50–80%, more or less in agreement with what was found already by Lorente et al. [RD17]. The magnitude of the surface anisotropy which is present in the TROPOMI surface DLER is therefore quite substantial.

At 670 and 463 nm the surface anisotropy parameter over vegetation is much lower than at 772 nm. This is partly caused by the fact that the surface albedo at these wavelength bands is also much lower than at 772 nm. Nevertheless, the percentages are also smaller than at 772 nm, in the range of 20–50%. For desert areas the anisotropy parameter is slightly smaller at 670 and 463 nm than at 772 nm. However, the percentages are similar for all three wavelength bands, about 10–20%. For 463 nm the values are slightly smaller, though. This is probably because of increased Rayleigh scattering at the shorter wavelength, which results in a more diffuse illumination of the surface and in more diffuse transport of light in the atmosphere.

10.2 MODIS surface BRDF

The MODIS Ross–Li surface BRDF model is a linear kernel-based BRDF model used to describe the surface reflectance of land surfaces. The surface anisotropy is described by two geometry-dependent kernels, which have to be combined with the provided kernel coefficients if one wants to calculate the BRDF. The Li–Sparse kernel K_{geo} is the geometric kernel, which describes the contribution of sunlit and shaded parts of a scene due to the presence of three-dimensional object, typically trees. The Ross–Thick kernel K_{vol} is the volumetric kernel, which describes the smaller-scale variation of the leaf canopy, i.e., the orientation of the leafs themselves.

The geometric and volumetric kernels are independent on wavelength. The wavelength dependence of the BRDF is contained entirely in the kernel coefficients. The expression for the surface reflectivity is [RD23]:

$$A_{\mathrm{g}}(\lambda, \theta, \theta_0, \phi - \phi_0) = f_{\mathrm{iso}}(\lambda) + f_{\mathrm{vol}}(\lambda) \cdot K_{\mathrm{vol}}(\theta, \theta_0, \phi - \phi_0) + f_{\mathrm{geo}}(\lambda) \cdot K_{\mathrm{geo}}(\theta, \theta_0, \phi - \phi_0) \qquad (1)$$

The exact expressions needed to calculate K_{vol} and K_{geo} are provided in Appendix A. The three coefficients $f_{iso}, f_{vol}, f_{geo}$ are the kernel coefficients of the isotropic, volumetric, and geometric contributions. These kernel coefficients are stored in the MODIS MCD43C2 v6.1 product [ER6] that we used for the validation.

10.3 Validation approach

To be able to compare TROPOMI surface DLER and MODIS surface BRDF we first need to define the viewing and solar angles that are involved. We start out with an artificial array of viewing angles θ_{v} which range
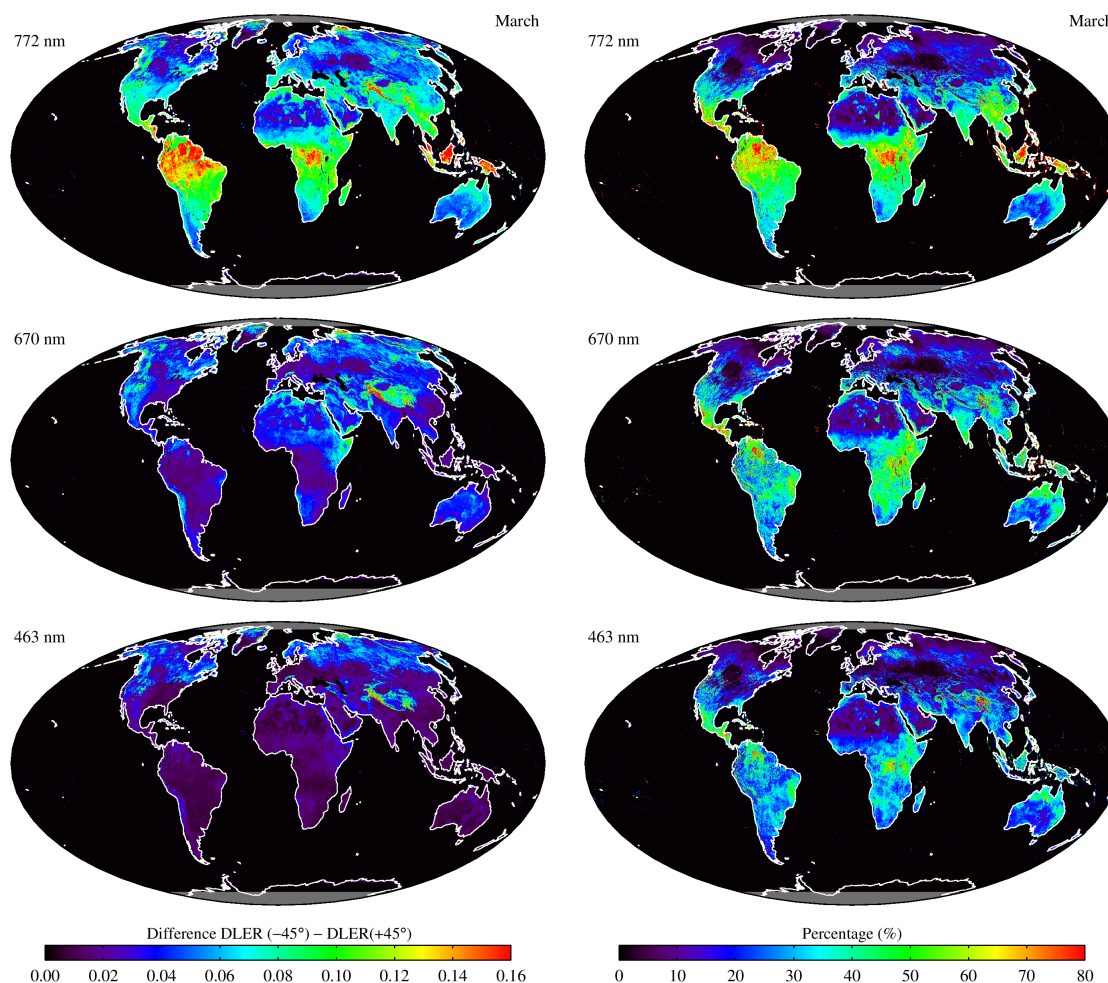
Figure 20: Left: Surface anisotropy parameter, defined as the DLER at a viewing angle of –45° ("East") minus the DLER at viewing angle +45° ("West"). Right: The same, but now as percentage of the MIN-LER.

between –66.3° and +66.3° in 101 steps, where the minus sign indicates an east viewing direction and the plus sign indicates a west viewing direction. Already this definition of θ_v is enough to calculate the TROPOMI DLER for any of the grid cells inside the TROPOMI surface DLER field.

Finding the complete set of angles needed for calculating MODIS surface BRDF (θ, θ_0, $\phi - \phi_0$) is a bit more complicated. For every artificial θ_v of the grid cell at hand we determine the associated solar zenith angle θ_0 and relative azimuth angle $\phi - \phi_0$. This is done on the basis of the TROPOMI viewing and solar geometry from a TROPOMI orbit of the same day, using only θ_v and the central latitude of the grid cell as input. The viewing zenith angle θ is by definition the absolute value of θ_v. In other words: $\theta = |\theta_v|$. With all three angles known, the kernels K_{vol} and K_{geo} can be calculated using the equations provided in Appendix A. The kernel coefficients f_{iso}, f_{vol}, f_{geo} are then determined from the MODIS MCD43C2 product [ER6] of the given day. After that, the MODIS surface BRDF can then be calculated according to equation (1).

10.4   Results

In this section some of the validation results are presented. We present results for seven regions:

1. Libyan desert (25–29°N ; 23–27°E)

2. Amazonian rainforest (5–15°S ; 55–65°W)

3. Equatorial Africa (1–7°S ; 17–29°E)

4. Sahara desert (16–20°N ; 11–15°E)

5. Australia (21–30°S ; 121–143°E)

6. Northern Africa (16–29°N ; 8–30°E)

7. North America (31–39°N ; 85–100°W)

The results were obtained for 15 February 2019. This means that the MODIS MCD43C2 product from 15 February 2019 was used, and that calendar month February from the TROPOMI DLER database was used.

10.4.1 Case 1: Libyan desert

Figure 21 presents results for the Libyan desert. In the left panel the vertical axis presents the (non-directional) TROPOMI surface LER at 670 nm. The horizontal axis presents the MODIS surface BRDF derived from MODIS band 1, which is centred around 645 nm. Different colours are used for different viewing angles θ_v. For east viewing directions the colours are blue, for west viewing directions the colours are red (see colour bar in the plot window). Because the TROPOMI surface LER is not dependent on the viewing angle θ_v, we see horizontal lines of constant LER. Already the TROPOMI LER shows a fair agreement with the MODIS BRDF. In the right panel the improved (directional) TROPOMI surface DLER is presented on the vertical axis. Since the DLER database does contain the directional dependence, the agreement is now much better.
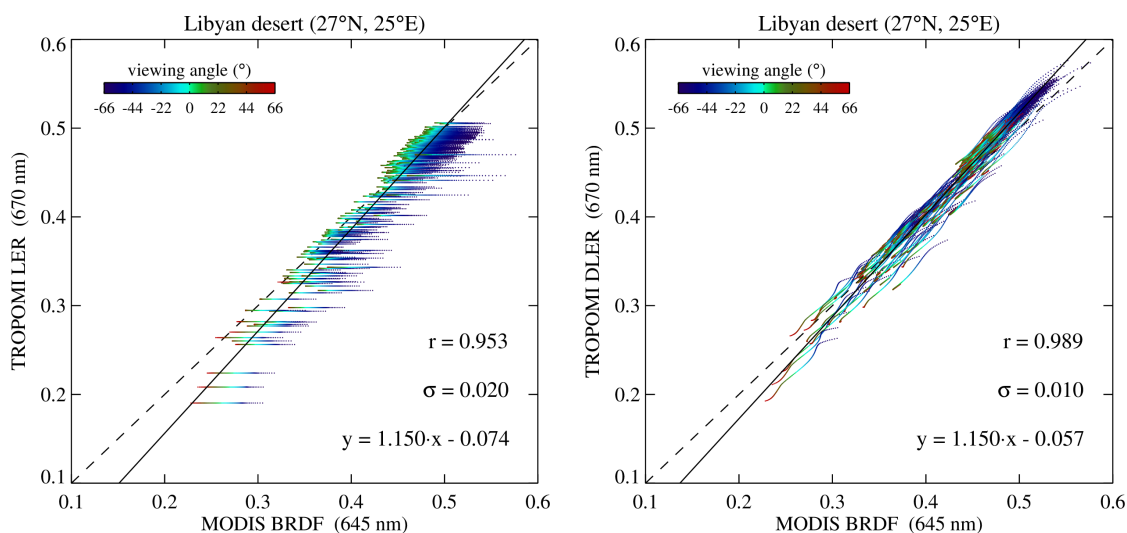

Figure 21: Left: TROPOMI surface LER versus MODIS surface BRDF for a region in the Libyan desert. The simulated case is for 15 February 2019. Right: The same type of plot, but now TROPOMI surface DLER is presented on the vertical axis. MODIS band 1 is centred around 645 nm.

The better performance is expressed by Pearson's correlation coefficient r, which increased from 0.953 to 0.989. The black lines represents linear fits to the data points. In the right panel, the coefficients of the linear fit are closer to the coefficients of the one-to-one relationship (indicated by the dashed line). The parameter σ, defined as the standard deviation of the data points w.r.t. the linear fit, decreased from 0.020 to 0.010. The obvious conclusion is that the DLER performs better than the standard LER for this particular region.

Please note, however, that the absolute numbers of the linear fit are hard to interpret, because there is a wavelength difference between the TROPOMI wavelength band and the MODIS band. Surface reflection is wavelength dependent. Also, DLER and BRDF are not the same parameters, as explained in section 7 of the ATBD [RD16]. Nevertheless, the fact that the slope of the linear fit (1.150) is too high can be partly explained by the fact that the surface reflection at 670 nm is higher than at 645 nm for desert surface types.

10.4.2 Case 2: Amazonian rainforest

Figure 22 presents the results for a region in the Amazonian rainforest. This time we present results for the 2314-nm TROPOMI DLER wavelength band, which is compared to MODIS BRDF from band 7, which is centred around 2130 nm. The difference in wavelength prevents a fully quantitative comparison, but the outcome of the comparison is relevant nevertheless.
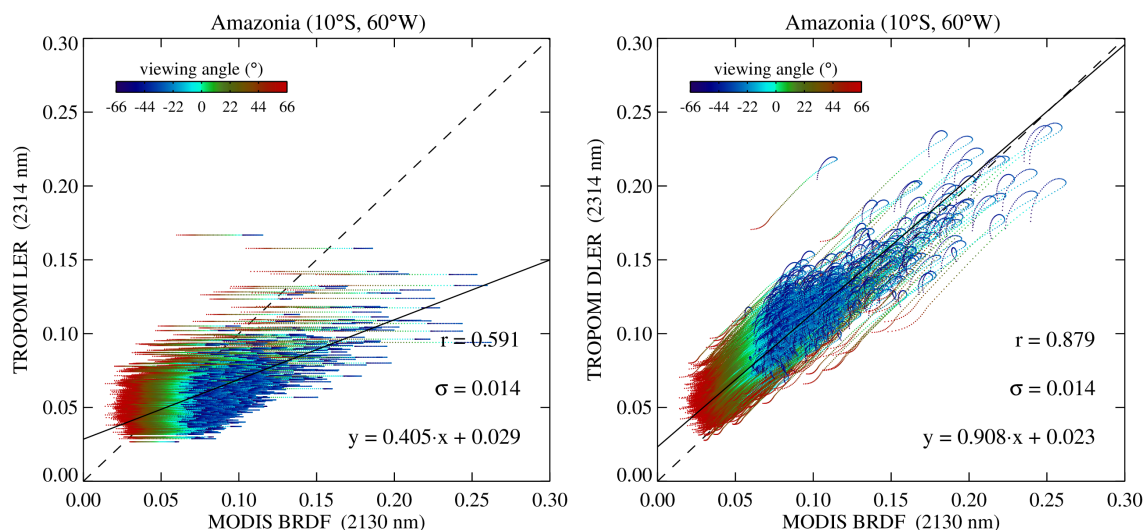
Figure 22: Left: TROPOMI surface LER versus MODIS surface BRDF for a region in the Amazonian rainforest. Right: The same plot, but now with TROPOMI surface DLER on the vertical axis.

In the left panel of Figure 22 the agreement between TROPOMI LER and MODIS BRDF is fair, but not much more than that. The Pearson correlation coefficient is 0.591, indicative of a low correlation. The linear fit is deviating quite a lot from the one-to-one relationship. In the right panel of Figure 22, the agreement between TROPOMI DLER and MODIS BRDF is quite good. Pearson's correlation coefficient r now amounts to 0.879, indicating high correlation, and the slope of the linear fit is much closer to one. The intercept of the linear fit may be explained by the large difference in wavelength, which prevents a quantitative comparison.

10.4.3 Case 3: Equatorial Africa

Figure 23 presents a validation result for a vegetated region in equatorial Africa. This time we present results for the 772-nm TROPOMI DLER wavelength band, which is compared to MODIS surface BRDF from band 2, which is centred around 859 nm. The large difference in wavelength again prevents a quantitative comparison, but differences in surface reflection due to the wavelength difference are not excessive. In the left panel of Figure 23 we see a rather reasonable agreement between TROPOMI surface LER and MODIS surface BRDF. However, Pearson's correlation coefficient r is 0.468, indicating a low correlation. This lack of correlation is a
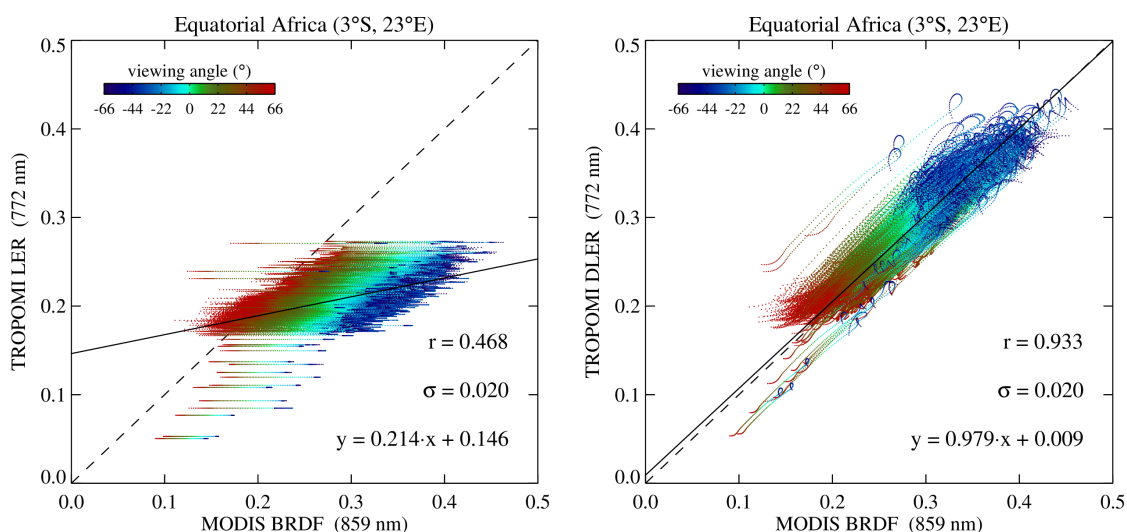

Figure 23: Left: TROPOMI surface LER versus MODIS surface BRDF for a vegetated region in Equatorial Africa. Right: The same plot, but now with TROPOMI surface DLER on the vertical axis.

direct result of the absence of a directional dependence in the TROPOMI surface LER database in combination with the large anisotropy of the (vegetated) surface.

In the right panel of Figure 23 we see a good correlation between TROPOMI DLER and MODIS BRDF. The Pearson's correlation coefficient r now amounts to 0.933, indicative of a high correlation. The standard deviation σ remained more or less the same but the linear fit is now quite close to the one-to-one relationship. The intercept is very close to zero and the slope is only slightly smaller than one. The DLER database performs, therefore, much better than the LER database.

10.4.4   Case 4: Sahara desert

The case shown in Figure 24 is that of a region in the southern part of the Sahara desert. The DLER wavelength band studied is the 772-nm wavelength band, which is compared with MODIS band 2, which is centred around 859 nm. Already for the TROPOMI LER database (left panel) there is a good agreement with the MODIS BRDF product, at least, when taking into account that there is a difference in wavelength. The correlation coefficient r is 0.921, indicating high correlation. The spread, indicated by the standard deviation σ, is 0.019, which is quite low considering the high values of BRDF that are reached. Still, in the right panel the TROPOMI DLER does better. Pearson's correlation coefficient now amounts to 0.959, and σ went down to 0.014. The linear fit did not improve much. The slope of 0.979 is partly explained by the difference in wavelength: for desert surfaces the surface albedo increases with increasing wavelength.
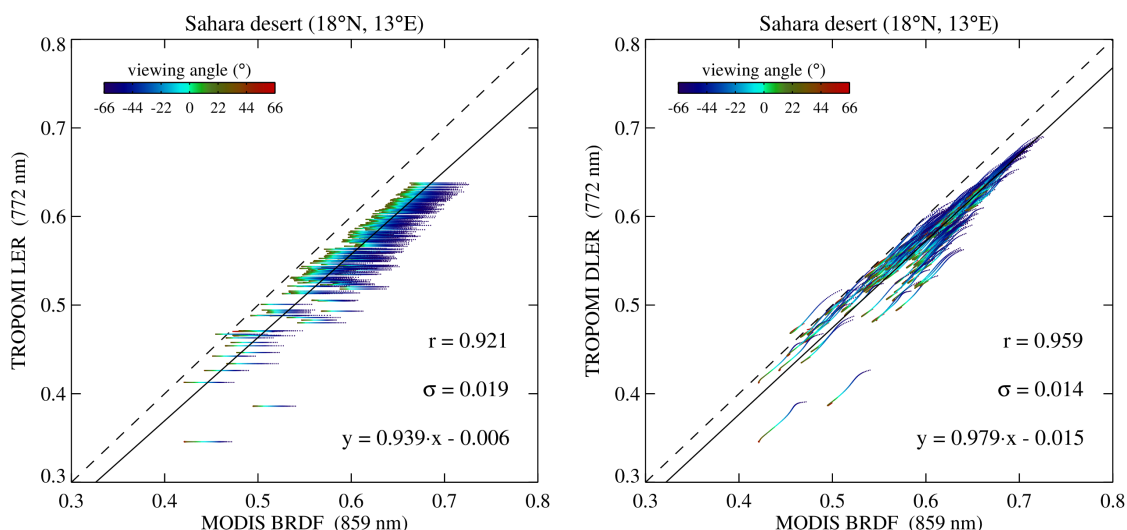

Figure 24: Left: TROPOMI surface LER versus MODIS surface BRDF for a region in the southern Sahara desert. Right: The same plot, but now with TROPOMI surface DLER on the vertical axis.

10.4.5   Case 5: Australia

Figure 25 presents the results at 670 nm for a region in Australia. Already for the TROPOMI surface LER (left window) we find a fair agreement. The region that was selected is relative large (see section 10.4) and the variability in surface LER values is also large. This explains why the correlation is already quite good, with a Pearson correlation coefficient of 0.899. However, the neglect of directionality in the surface LER is also evident. The result for the TROPOMI surface DLER (right window) shows a clear improvement. Pearson's correlation coefficient went up to 0.938 and the standard deviation σ, indicating the spread of the data points around the linear fit, went down from 0.021 to 0.017. The linear fit is now closer to the one-to-one relationship, and, although it is not perfect yet, for most data points the DLER is closer to the BRDF than the LER is.

10.4.6   Case 6: Northern Africa

Figure 26 presents the results for a region in the northern part of the African continent. The region that was selected is again relatively large, so the spread in the surface LER values is also very large. The values range between 0.1 and 0.6, which indicates that both vegetated and desert surfaces are included in the selected
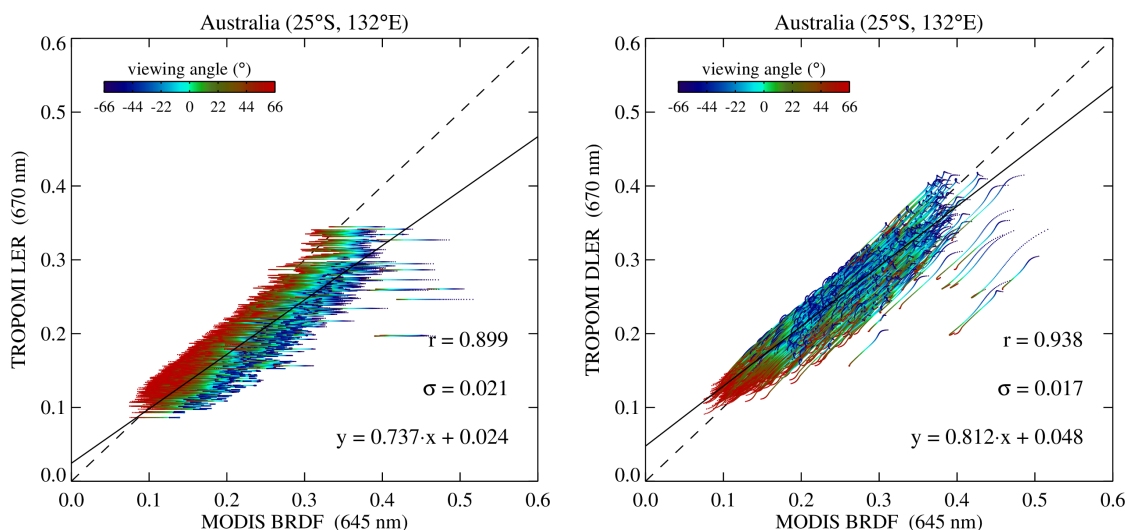
Figure 25: Left: TROPOMI surface LER versus MODIS surface BRDF for a region in Australia. Right: The same plot, but now with TROPOMI surface DLER on the vertical axis.
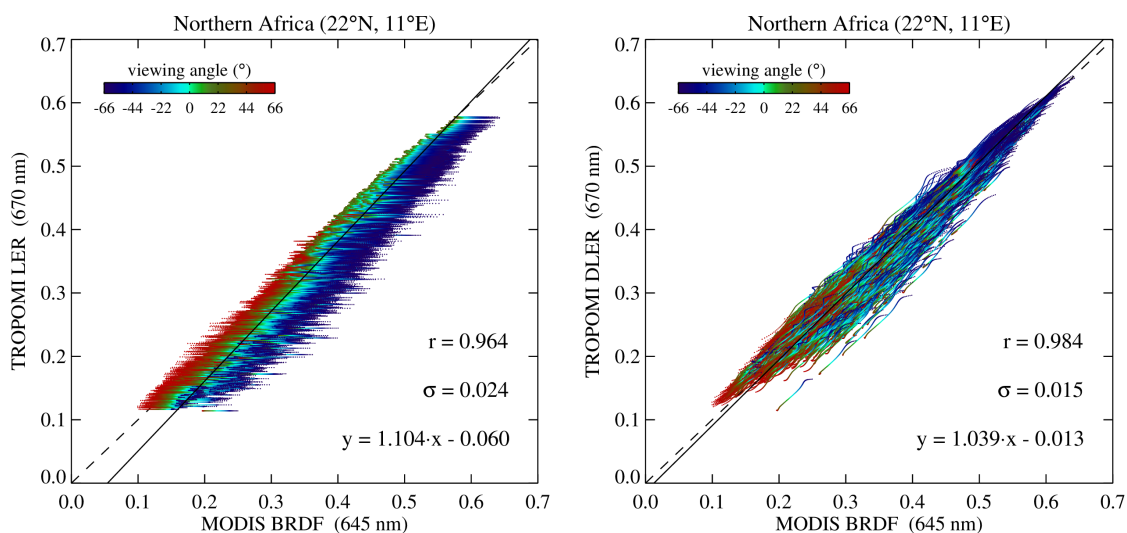

Figure 26: Left: TROPOMI surface LER versus MODIS surface BRDF for a region in the northern part of Africa. Right: The same plot, but now with TROPOMI surface DLER on the vertical axis.

region. The TROPOMI surface LER at 670 nm has a good correlation with the MODIS BRDF at 645 nm (left window). In the right window of Figure 26 the DLER results are shown. The correlation improved even further, with Pearson's correlation coefficient going from 0.964 to 0.984. The standard deviation σ went down from 0.024 to 0.015 and the linear fit to the data points is closer (very close) to the one-to-one relationship.

10.4.7   Case 7: North America

Figure 27 presents the results at 670 nm for a region in North America. Despite that fact that the selected region is again relatively large, the range in surface LER is fairly limited. The surface of the selected region is mostly covered by vegetation. The left window of Figure 27 shows the performance of the TROPOMI surface LER. The correlation with MODIS BRDF at 645 nm is reasonable. The TROPOMI surface DLER, however, does a lot better in the right window of Figure 27. The Pearson correlation coefficient went up from 0.872 to 0.969, indicating a very good correlation. The standard deviation σ went down from 0.012 to 0.007 and the linear fit is clearly much closer to the one-to-one relationship compared to the situation in the left window.
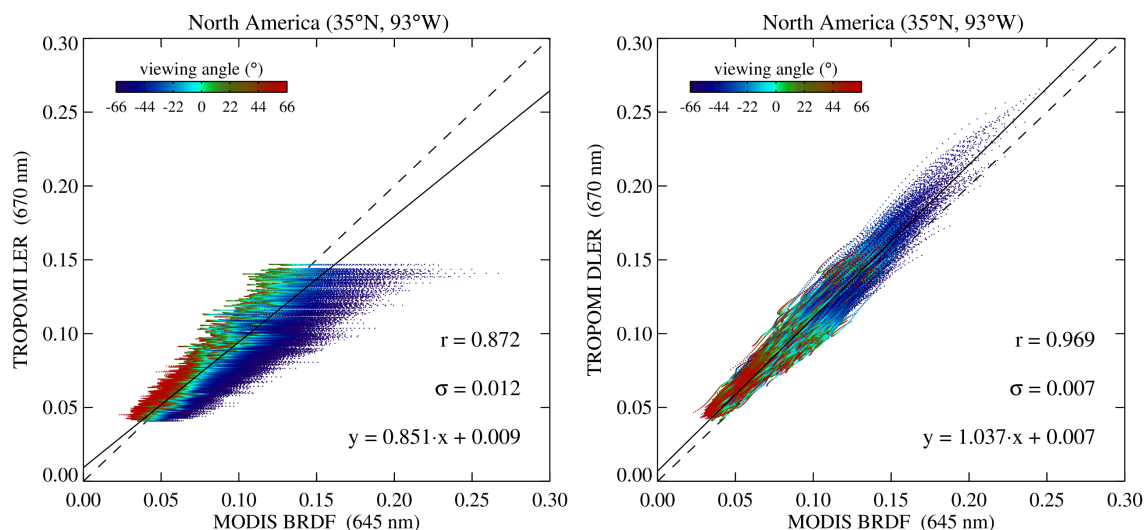
European Space Agency
Agence spatiale européenne

Figure 27: Left: TROPOMI surface LER versus MODIS surface BRDF for a region in North America. Right: The same plot, but now with TROPOMI surface DLER on the vertical axis.

10.5   Summary

The validation that was presented in this section was mostly focused on the directional behaviour of the TROPOMI DLER database. Quantitative validation is difficult because of wavelength differences between the MODIS bands and the TROPOMI DLER wavelength bands. The agreement is best for the wavelength band at 670 nm, for which the nearby MODIS band 1 can be used as a reference. Overall, the results that were presented in section 10.4 indicate that the improvement in going from LER to DLER is the largest for vegetated surfaces. This is as expected, because vegetated surfaces show the strongest surface anisotropy to begin with (see, for instance, Figure 20). But also for desert regions the improvements are clear. In all seven cases that were presented the correlation, measured by Pearson's correlation coefficient, increased and the linear fit moved closer towards the one-to-one relationship. The standard deviation σ, indicating the spread of the data points around the linear fit, went down in all cases as well, to typical values of 0.01–0.02.

The improvement achieved by the DLER (with respect to the LER) depends strongly on the scattering geometry. The maximum improvement can be estimated easily from Figures 21 to 27. For instance, for the Libyan desert, maximum improvements of $\sim$0.08 (or 20%) are achieved at 670 nm. For the vegetated surface of equatorial Africa, maximum improvements of up to 0.2 are seen at 772 nm, which corresponds to 50–100%. These numbers are confirmed by Figure 20. In conclusion, the TROPOMI surface DLER is an important improvement on the traditional TROPOMI surface LER database.

European Space Agency
Agence spatiale européenne

11 Conclusion

The TROPOMI surface DLER climatology is constantly being improved, so the results only reflect the quality for the database version which was studied. The version of the database that was studied is version 2.0.

The validation study relied on two types of intercomparisons. First, the non-directional TROPOMI surface LER database was compared with the heritage surface LER databases based on the OMI, SCIAMACHY, and GOME-2 instruments. The main conclusion here is that there is good agreement. For previous versions of the TROPOMI surface LER database (up to version 1.2), deviations were found which could be linked to radiometric calibration errors in the TROPOMI L1 product. These calibration errors had been confirmed [RD24] in the past but new collection-3 TROPOMI L1 data are not troubled by these calibration problems. Since the TROPOMI surface DLER database is based on these new collection-3 TROPOMI L1 data, the deviations that were found in earlier versions have disappeared.

For the longer wavelength bands (670 to 2314 nm) the TROPOMI surface LER is biased below 0.003 and the requirements (0.02+10% for $\lambda > 600$ nm, see [RD18]) are met easily. For the shorter wavelength bands (328 to 494 nm) the TROPOMI surface LER is biased up to 0.02 and the requirements (0.03+10% for $\lambda < 500$ nm) are met relatively easily.

In a second validation step, the directional TROPOMI surface DLER database was compared to MODIS surface BRDF. This comparison was focused on testing the directionality of the DLER database and can only be done reliably for the 670 nm wavelength band. Ccomparisons at 772 and 2314 nm were presented, but only analysed qualitatively. The current version (v2.0) of the database performs slightly better than the previous version (v1.0) of the database. This does not change the conclusion that was drawn already for version 1.0 of the database. The conclusion is that the DLER is able to capture the surface anisotropy very well. As a result, the TROPOMI DLER database is a large improvement on the TROPOMI LER database.

A Kernels for the Ross–Li BRDF model

This appendix lists the equations needed to calculate the kernels that make up the Ross–Li BRDF model of surface reflectance. Proper derivations of the Ross–Thick and Li–Sparse kernels can be found in [RD25].

A.1 Ross–Thick volumetric kernel

The Ross–Thick volumetric scattering kernel is defined in the following way [RD26]:

$$K_{\text{vol}} = \frac{(\pi/2 - \xi)\cos\xi + \sin\xi}{\cos\theta + \cos\theta_0} - \frac{\pi}{4} \;. \tag{2}$$

In equation (2), θ refers to the viewing zenith angle and θ_0 to the solar zenith angle. The angle ξ is defined as

$$\cos\xi = \cos\theta\cos\theta_0 + \sin\theta\sin\theta_0\cos(\psi - \psi') \;, \tag{3}$$

where ψ and ψ' are the viewing and solar azimuth angles following the definition in [RD23]. Exact backscattering ($\xi = 0°$) occurs for $\psi - \psi' = 0°$, which agrees with the definition used for the TROPOMI data products.

A.2 Li–Sparse geometric kernel

The Li–Sparse geometric scattering kernel [RD27] is defined as:

$$K_{\text{geo}} = O - \sec\theta^\star - \sec\theta_0^\star + \frac{1}{2}(1 + \cos\xi^\star)\sec\theta^\star\sec\theta_0^\star \;. \tag{4}$$

The term O in equation (4) and the starred angles $\theta^\star$, $\theta_0^\star$, and $\xi^\star$ are calculated using the following set of equations:

$$\theta^\star = \arctan\left(\frac{b}{r}\tan\theta\right) \;, \quad \theta_0^\star = \arctan\left(\frac{b}{r}\tan\theta_0\right) \;, \tag{5}$$

$$\cos\xi^\star = \cos\theta^\star\cos\theta_0^\star + \sin\theta^\star\sin\theta_0^\star\cos(\psi - \psi') \;, \tag{6}$$

$$O = \frac{1}{\pi}(t - \sin t\cos t)(\sec\theta^\star + \sec\theta_0^\star) \;, \tag{7}$$

$$\cos t = \frac{h}{b}\frac{\sqrt{D^2 + (\tan\theta^\star\tan\theta_0^\star\sin(\psi - \psi_0))^2}}{\sec\theta^\star + \sec\theta_0^\star} \;, \tag{8}$$

$$D = \sqrt{\tan^2\theta^\star + \tan^2\theta_0^\star - 2\tan\theta^\star\tan\theta_0^\star\cos(\psi - \psi')} \;. \tag{9}$$

The parameters b/r and h/b are the crown relative shape and the crown relative height, respectively. These were fixed to 1 and 2, respectively, following [RD23].